QATAR UNIVERSITY

COLLEGE OF ENGINEERING

AUTOMATED SEGMENTATION OF CEREBRAL ANEURYSM USING A NOVEL STATISTICAL MULTIRESOLUTION APPROACH

BY

YOUSRA MOUNIR REGAYA

A Thesis Submitted to
the Faculty of the College of
Engineering
in Partial Fulfillment
of the Requirements
for the Degree of
Master of Science in Computing

January 2018

Committee

The members of the committee approve the Thesis of YOUSRA MOUNIR REGAYA defended on December 11^{th}, 2017:

Prof. Abbes Amira

Thesis Supervisor

Dr. Noor Al-Maadeed

Thesis Co-Supervisor

Prof. Fatih Kurugollu

Committee Member

Dr. Uvais Qidwai

Committee Member

Approved:

Dr. Khalifa Al-Khalifa, Dean, COLLEGE OF ENGINEERING

Abstract

Regaya, Yousra, M., Masters:

January: 2018, Master of Science in Computing

Title: Automated Segmentation of Cerebral Aneurysm Using a Novel Statistical Multiresolution Approach

Supervisor of Thesis: Prof. Abbes Amira

Cerebral Aneurysm (CA) is a vascular disease that threatens the lives of many adults. It affects almost $1.5 - 5\%$ of the general population. Sub-Arachnoid Hemorrhage (SAH), resulted by a ruptured CA, has high rates of morbidity and mortality. Therefore, radiologists aim to detect it and diagnose it at an early stage, by analyzing the medical images, to prevent or reduce its damages.

The analysis process is traditionally done manually. However, with the emerging of the technology, Computer-Aided Diagnosis (CAD) algorithms are adopted in the clinics to overcome the traditional process disadvantages, as the dependency of the radiologist's experience, the inter and intra observation variability, the increase in the probability of error which increases consequently with the growing number of medical images to be analyzed, and the artifacts added by the medical images' acquisition methods (i.e., MRA, CTA, PET, RA, etc.) which impedes the radiologist' s work.

Due to the aforementioned reasons, many research works propose different segmentation approaches to automate the analysis process of detecting a CA using complementary segmentation techniques; but due to the challenging task of developing a robust reproducible reliable algorithm to detect CA regardless of its shape, size, and location from a variety of the acquisition methods, a diversity of proposed and developed approaches exist which still suffer from some limitations.

This thesis aims to contribute in this research area by adopting two promising techniques based on the multiresolution and statistical approaches in the Two-Dimensional (2D) domain. The first technique is the Contourlet Transform (CT), which empowers the segmentation by extracting features not apparent in the normal image scale. While the second technique is the Hidden Markov Random Field model with Expectation Maximization (HMRF-EM), which segments the image based on the relationship of the neighboring pixels in the contourlet domain.

The developed algorithm reveals promising results on the four tested Three-Dimensional Rotational Angiography (3D RA) datasets, where an objective and a subjective evaluation are carried out. For the objective evaluation, six performance metrics are adopted which are: accuracy, Dice Similarity Index (DSI), False Positive Ratio (FPR), False Negative Ratio (FNR), specificity, and sensitivity. As for the subjective evaluation, one expert and four observers with some medical background are involved to assess the segmentation visually. Both evaluations compare the segmented volumes against the ground truth data.

Dedication

To my beloved parents

The reason of my existence and persistence

To my brother and sisters

My parents' precious gift

To my second family

Who hosted me generously and me with love

To Imene, Zeineb, and Abeer

Who supported me throughout the journey and endured my temper

Acknowledgements

First and foremost, I would like to express my sincere gratitude to my supervisor Prof. Abbes Amira for his insightful advise, guidance, support, and encouragement through the learning and working journey of this master thesis.

Moreover, I would like to acknowledge my co-supervisor Dr. Noor Al Maadeed for her efforts and her valuable feedback. I would like also to thank Dr. Sarada P. Dakua from Hamad Medical Cooperation (HMC) for his support, provision of the datasets, and commitment to fulfill this research work. Furthermore, I would like to thank Dr. Rabaa Youssef for her valuable advise. Furthermore, I wish to acknowledge Dr. Pablo García-Bermejo from HMC for his help in the subjective evaluation.

Finally, my deepest gratitude to my family and friends who had faith and confidence in me to fulfill this work and supported me during my entire life.

Table of Contents

List of Tables

List of Figures

List of Algorithms

Author's Publications

Submitted Journals

- Yousra M. Regaya, Abbes Amira, Sarada P. Dakua, Noor A. Al-Maadeed, Pablo García-Bermejo, and Julien Abinahed, "Automated Segmentation for Cerebral Aneurysm using Multiresolution Statistical Approaches", Submitted to Computerized Medical Imaging and Graphics.

- Yousra M. Regaya, Abbes Amira, Sarada P. Dakua, Noor A. Al-Maadeed, and Julien Abinahed, "Cerebral Aneurysm Segmentation: Literature Review", Submitted to Medical Image Analysis.

List of Acronyms

CA	Cerebral Aneurysm
SAH	Sub-Arachnoid Hemorrhage
CTA	Computed Tomographic Angiography
MRA	Magnetic Resonance Angiography
TOF-MRA	Time-of-Flight Magnetic Resonance Angiography
CE-MRA	Contrast-Enhanced Magnetic Resonance Angiography
PC-MRA	Phase Contrast Magnetic Resonance Angiography
MRI	Magnetic Resonance Imaging
DCA	Diagnostic Cerebral Angiography
DSA	Diagnosis Subtraction Angiography
RA	Rotational Angiography
PET	Positron Emission Tomography
US	Ultrasound
CAD	Computer-Aided Diagnosis
MIS	Medical Image Segmentation
CT	Contourlet Transform

ICT	Inverse Contourlet Transform
HMRF	Hidden Markov Random Field
HMM	Hidden Markov Model
ROI	Region of Interest
2D	Two-Dimensional
3D	Three-Dimensional
SVM	Support Vector Machine
KNN	K-Nearest Neighbors
ANN	Artificial Neural Network
NB	Naive Bayes
ML	Maximum Likelihood
FCM	Fuzzy C-Means
EM	Expectation Maximization
PCA	Principle Component Analysis
MAP	Maximum a Posterior
FM	Finite Mixture
HWT	Haar Wavelet Transform
MRF	Markov Random Field
LBM	Lattice Boltzmann Model
LBGM	Lattice Boltzmann Geodesic Active Contour Method

MS-PCA	Multiscale Principle Component Analysis
POI	Points of Interest
PDFB	Pyramidal Directional Filter Bank
LP	Laplacian Pyramid
DFB	Directional Filter Bank
CSA	Clonal Selection Algorithm
GMM	Gaussian Mixture Model
FCEM	Fuzzy Clustering Expectation Maximization
CSA	Clonal Selection Algorithm
MCMC	Markov Chain Monte Carlo
MOE	Mean Overlap Error
RDE	Relative Distance Error
PSNR	Peek Signal to Noise Ratio
RMS	Root Mean Square
STD	Standard Deviation
ROC	Receiver Operating Characteristic
ARE	Average Relative Error
DSI	Dice Similarity Index
VD	Volume Difference
RAVD	Relative Absolute Volume Difference

TPR	True Positive Ratio
FPR	False Positive Ratio
FNR	False Negative Ratio
GAS	Geometric Active Surfaces
GAC	Geometric Active Contour
mm	millimeters
AD	Average Distance
JM	Jaccard's Measure
AR	Aspect Ratio
VR	Volume Ratio
HD	Hausdorff Distance
ASD	Absolute Surface Distance
MASD	Mean Absolute Surface Distance
TP	True Positive
TN	True Negative
FP	False Positive
FN	False Negative
MCE	Miss-classification Error
E-Step	Expectation Step
M-Step	Maximization Step

sec	seconds
min	minutes
DICOM	Digital Imaging and Communications in Medicine
STL	STereoLithography
HMC	Hamad Medical Corporation
FPGA	Field-Programmable Gate Array
GPU	Graphics Processing Unit

Chapter 1: Introduction

This chapter provides an insight of the overall picture of this thesis. Section 1.1 introduces the motivation to tackle Cerebral Aneurysm (CA) segmentation problem. Section 1.2 highlights the problem statement; whilst Section 1.3 lists the objectives and contribution of this work. Finally, Section 1.4 provides the structure of this thesis.

1.1 Motivation

An aneurysm is a weak spot or a dilation in blood vessels. Such an abnormal formulation when it takes place in the brain, it is known as a cerebral aneurysm, an intracranial aneurysm, or a brain aneurysm. We will use the Cerebral Aneurysm (CA) terminology throughout this thesis.

CA appears most commonly in areas with high blood flow, more precisely at the branching point of the arteries [39, 58]. Per [11, 39], $1.5 - 5\%$ of the general population are affected by CA. It takes usually several years to develop; therefore, it is detected more commonly after the age of forty. Different causes may lead to this abnormality formulation as a constant blood flow pressure, infections, drugs, direct brain trauma caused by an accident, etc. Figure 1.1, adapted from [39], illustrates the different status of the brain blood vessels: healthy vessels, the formulation of an unruptured CA, and the formulation of a ruptured CA.

Usually, a small CA (less than 5 millimeters) is asymptomatic [39]. As an

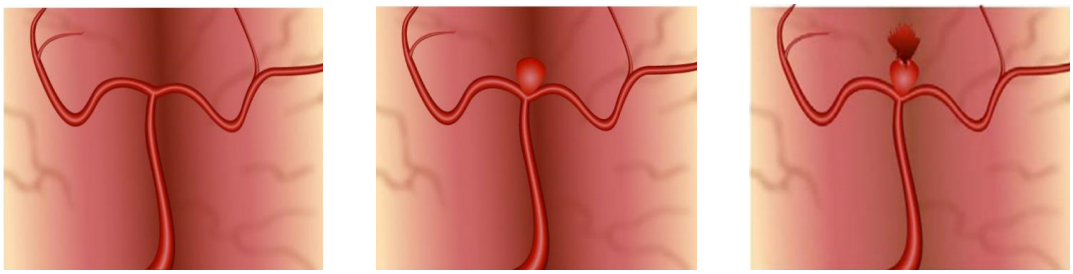

(a) (b) (c)

Figure 1.1: Different status of brain blood vessels: (a) healthy vessels (b) CA formulation (c) ruptured CA [39]

aneurysm enlarges gradually, taking some size and shape, the membrane becomes weaker. This growth produces more pressure affecting consequently the brain and the surrounding nerves. Over time, this pressure and even strong emotions may cause the rupture of a CA, resulting in the blood leakage into the sub-arachnoid space. This incident is known medically as the Sub-Arachnoid Hemorrhage (SAH), which has high rates of morbidity and mortality. Different damages to the brain tissues and functions may happen consequently depending on the amount of blood loss that leads to different symptoms (e.g., sudden severe headache, nausea and vomiting, vision impairment, hemorrhage stroke, drowsiness, coma, or death as a worst-case scenario). Figure 1.2 illustrates some statistics regarding the damages that could be caused by a ruptured aneurysm, where $30 - 40\%$ of the patients having a ruptured CA die [39]. Therefore, detecting, diagnosing, and treating patients with a CA at an early stage is an urgent matter to prevent more damages or reduce the high rates of morbidity and mortality.

A clinician initiate the process by analyzing the medical images acquired from a suitable adopted acquisition method (or modality), as each one captures different quantitative and qualitative information; for CA's detection and analysis, the most suitable modalities are Computed Tomographic Angiography (CTA),

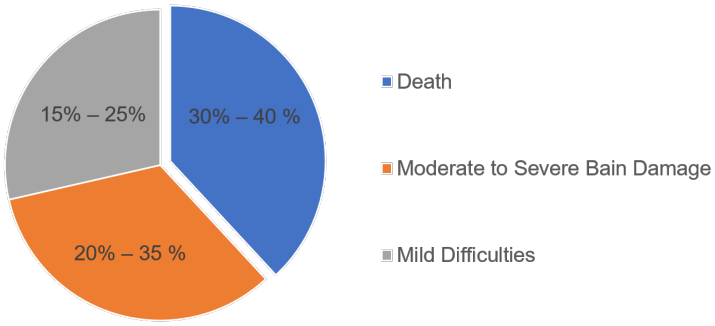

Figure 1.2: Statistics of ruptured CA damages

Magnetic Resonance Angiography (MRA), Diagnostic Cerebral Angiography (DCA), and Rotational Angiography (RA) [67, 86]. Later, according to a clinician' s diagnosis of the acquired images, the best suitable treatment is selected accordingly. Globally, four therapeutic options are available [11, 32], which are listed below. Moreover, Figure 1.3, adapted from [39, 45], illustrates the three recommended treatments when a large unruptured or ruptured CA is detected and diagnosed:

1. **Medical Therapy**: It is recommended when a small unruptured CA is detected. As a small aneurysm does not need to be treated unless a significant change is observed over time, a regular imaging examination is requested to follow up with the patient.

2. **Clipping**: It is an open neurosurgery, recommended when a large unruptured or ruptured CA is detected. In this treatment, a clip is placed around the base of an aneurysm to prevent the blood leakage.

3. **Coiling**: It is an interventional neuroradiology, recommended when a large unruptured or ruptured CA is detected too. In this treatment, a CA is treated inside the brain blood vessels by directing a tube, called a

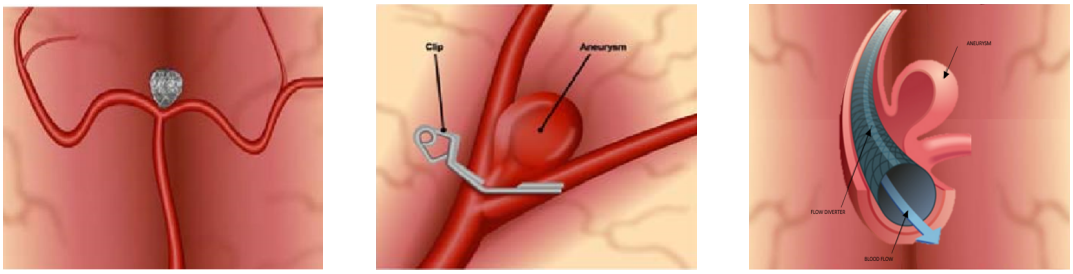

(a) (b) (c)

Figure 1.3: Three treatment options for a large and ruptured diagnosed CA: (a) Coiling (b) Clipping (c) Blood Flow Diverters [39, 45]

catheter, through the vessels into a CA to place soft platinum micro-coils that act as a mechanical barrier to the blood flow.

4. **Blood Flow Diverters**: It is recommended when a large unruptured or ruptured CA is detected as well. This treatment places a tube made of porous material within the CA. The porosity is increased at the two-ending point and decreased at the central point to block the entrance of the blood to the area of a CA.

1.2 Problem Statement

Medical image analysis is an imperative task in order to detect and determine any abnormality that explains a person's symptoms, where the best treatment is selected according to the diagnosis results.

Traditionally, the analysis step is done manually by a clinician. This procedure suffers from many disadvantages as the introduced artifacts by the acquisition devices/scanners which impede a clinician' s work, the bias results depending on a clinician' s experience, and the significant increase in the number of images to be analyzed which increases consequently the following: the probability of the analysis error, time consumption, and the number of needed experts. Due

to the aforementioned reasons, Computer-Aided Diagnosis (CAD) algorithms, known as Medical Image Segmentation (MIS) algorithms, are introduced to overcome the inter and intra operator variability, reduce the time consumption, offer reproducibility, and improve the accuracy. Accordingly, many segmentation algorithms are developed to analyze medical images, acquired from different modalities, to detect and diagnose different diseases including the CA disease.

CA segmentation algorithms help in determining the aneurysm state: ruptured or unruptured. Moreover, they help to determine the size (e.g., small, medium, or giant), the location (circle of Willis, anterior, or posterior), and the morphology (e.g., the neck length, dome height, and diameter) of a CA. Recently, these algorithms help also in measuring and analyzing the CAs' hemodynamics. All of the mentioned analysis helps a clinician in the treatment planning. Therefore, the high accuracy of a CA segmentation algorithm is very critical as it impacts greatly the clinician's decision, which affects directly the human life.

In the literature, different CA segmentation approaches are proposed, where each algorithm consists of complementary segmentation techniques selected carefully according to the adopted: dimensionality, modality, and the intended level of user interaction. However, each work suffers from some limitations which prevent to achieve the desired goal; these limitations are discussed later on in section 2.2.

1.3 Research Objectives and Contribution

As aforementioned in section 1.2, the existing CA segmentation algorithms suffer from a variety of limitations (e.g., inconsistent performance, the need for some human interactions, and applicable for some certain cases as giant

CAs only or for some certain types as saccular CAs only). Therefore, the main objective of this work is to contribute to this research area by:

1. Carrying out an intensive literature review with in-depth critical analysis of different MIS techniques and different existing CA segmentation algorithms.

2. Developing a new promising robust automatic CA segmentation algorithm using multiresolution and statistical approaches.

3. Evaluating the developed algorithm, given the ground truth data, objectively using well-known performance metrics (accuracy, Dice Similarity Index (DSI), False Positive Ratio (FPR), False Negative Ratio (FNR), sensitivity, and specificity) and subjectively by involving clinicians to assess the segmentation visually.

1.4 Thesis Organization

The remaining of this thesis is organized as follow: Chapter 2 introduces the three key concepts in this thesis by presenting their backgrounds and how they are addressed in the literature. These key concepts are MIS, CA, and the multiresolution and statistical approaches adopted in our proposed solution, which are presented in Sections 2.1, 2.2, and 2.3 respectively. Next, the methodology of the proposed solution is introduced and explained in Chapter 3. Later, the results of the objective and the subjective evaluation of the proposed algorithm are reported in Chapter 4. A conclusion and some future works are presented in Chapter 5. Finally, the tools used to investigate and visualize the segmented data in 2D and 3D domains are provided in the appendix.

Chapter 2: Background and Related Work

This chapter is concerned primarily to introduce the basic key concepts in this work. Section 2.1 introduces the Medical Image Segmentation (MIS) by addressing the following questions: What is it?, What are the different existing techniques?, and How they are adopted in the literature? Section 2.2 surveys the state-of-the-art of Cerebral Aneurysm (CA) segmentation algorithms, which is the problem tackled in this work. Later, in Section 2.3, we go deeper by introducing the multiresolution and statistical approaches adopted in the proposed solution and how they are addressed in the literature.

2.1 Medical Image Segmentation

MIS partitions the image pixels in Two-Dimensional (2D) domain, or voxels in Three-Dimensional (3D) domain, into distinct regions to distinguish between different existing anatomical structures; thereby, it separates between the Region of Interest (ROI) and the other components. This fundamental approach is introduced to help in the analysis of medical images, since decades, in order to detect the presence or the absence of some anomalies. This approach covers different biomedical applications as diagnosis, localization, treatment planning, computer integrated surgery, etc. The segmentation does not overtake the radiologists' role; it only provides a robust second opinion to help them at the analysis phase. Mathematically, MIS can be expressed by the following

equation 2.1

$$\bigcup S_k = I(x, y), \text{ where } S_{k_i} \cap S_{k_j} = \emptyset \tag{2.1}$$

, where $I(x, y)$ is an image and k is the number of partitioned regions in I [51]. MIS approaches can be classified according to the human intervention during the segmentation process into three main categories:

1. **Manual segmentation:** It is the traditional adopted technique. The radiologist has to go through the whole dataset, slice by slice, to select the ROI that best represents the region of the disease. This is a very tedious task as the acquired images include some artifacts introduced by the acquisition devices, known as modalities. Later, the ROI has to be carefully delineated. The accuracy of this step depends on the radiologist' s experience, which exposes the segmentation performance to inter and intra operator variability. For example, the same dataset segmented by different experts would most probably generate very different results [34].

2. **Semi-automatic segmentation:** It is the most commonly adopted approach in the literature. This category aims to combine both human expertise and computers to deal with the complexity of the task. The human intervention can be at one of the three following cases: initialize some parameters at the beginning of the algorithm, interact at some point while the algorithm is still running to give some sort of feedback, or stop the algorithm [34, 51].

   Meanwhile, the human intervention reduces the complexity of the task and produces effective segmentation results, it is still laborious and exposes the results to inter and intra operator variability as well.

3. **Automatic segmentation:** In this category, no human intervention is allowed at any point of the algorithm's running time. Indeed, a full

computerized algorithm is implemented to segment the medical images. The fact that humans have a high visual processing level but they still rely on an expert in the field to analyze these images, implies that developing such an algorithm with a high level of accuracy is an extremely challenging task. Therefore, until now full-automatic algorithms are restricted only to the research work and they are not yet adopted in the clinical practice [34].

A wide diversity of segmentation techniques are available, where usually they are not used separately. Complementary techniques are jointly employed to overcome the limitation of each individual technique [62, 80], which produce more accurate, robust, and effective segmentation to better analyze and diagnose different diseases. Indeed, these techniques are the main building blocks of any developed segmentation algorithm.

Initially, basic segmentation techniques are introduced as threshold-based, edge-based, and region-based where three main features are used to help in partitioning the image into distinct mutual exclusive regions: the distribution of pixels properties (intensity values or color), discontinuities in intensity levels, or finding distinct regions directly. These techniques resulted in a very naive segmentation which cannot cope with the complexity and the variations of anatomical structures, noise, cluttered objects and their different textures, variation in the illumination, etc. Therefore, these three techniques are usually used as an initial segmentation step. Consequently, artificial intelligence methods (e.g., pattern recognition and machine learning approaches) are introduced and used in conjunction with the basic techniques described above. However, these techniques tend to rely on the human intervention. Later on, while targeting full automatic approaches, experts' knowledge is implemented as models, atlas, etc [71].

The segmentation techniques are growing tremendously. Therefore, some form of organization is desirable to capture the breadth of these techniques.

Per [7, 33, 60, 62, 67, 92], MIS techniques can be categorized into seven groups, where Figure 2.13 summarizes all the available categories. Below each category is presented and described separately:

1. **Threshold-based:** These techniques identify an intensity value(s) as a threshold. Accordingly, image pixels whose values are less or equal to the defined threshold are grouped into one region, and all other pixels are grouped into a different region(s). Two threshold-based techniques exist: hard and multi-thresholding. The first technique fixes only one threshold value for the whole image. This technique is recommended when the intensity distribution of image pixels are sufficiently distinct. While in the second technique, many threshold values are determined over an image to overcome the limitation of the first technique when uneven background illumination is present. The threshold value(s) can be selected interactively for semi-automatic segmentation algorithms; as for the automatic segmentation algorithms, the automatic selection can be done by going through an iterative process to select the best-suited value(s). This automation increases the time complexity which increases with the size of the image [7]. The main objective of selecting the best suitable threshold value(s) is to minimize the error of assigning pixels to the wrong regions. This category is a simple yet a powerful technique. Nevertheless, it has its own limitations as the spatial information is not considerate, which exposes it to be subjective to noise. In addition, in its simplest techniques, hard-thresholding, it only identifies two regions. Moreover, this category cannot be adopted for multichannel images [62]. Figure 2.1 and 2.2 illustrate two segmentation examples of a Magnetic Resonance Imaging (MRI) human skull slice and a 3D RA CA slice using the two introduced threshold techniques respectively.

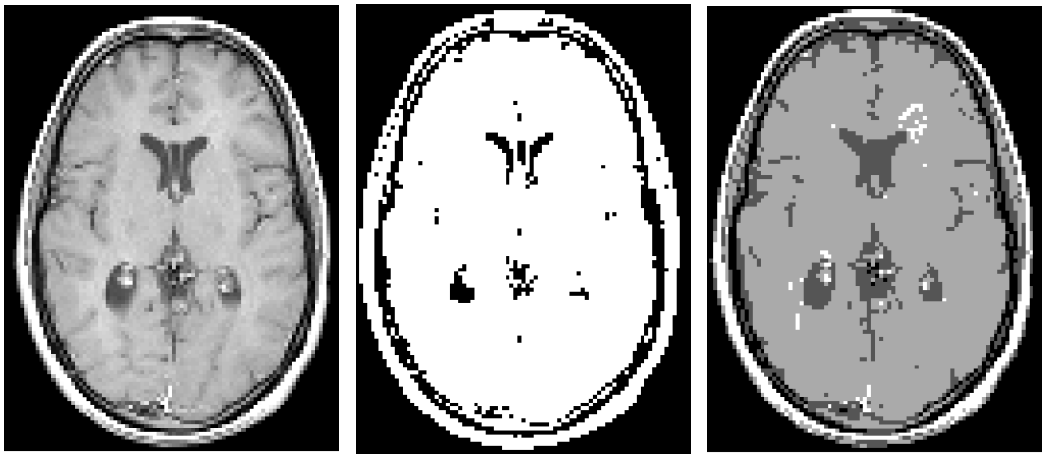

(a) (b) (c)

Figure 2.1: 128 × 128 MRI human skull slice (a) original gray-scale image (b) segmented image using hard-thresholding (c) segmented image using multi-thresholding

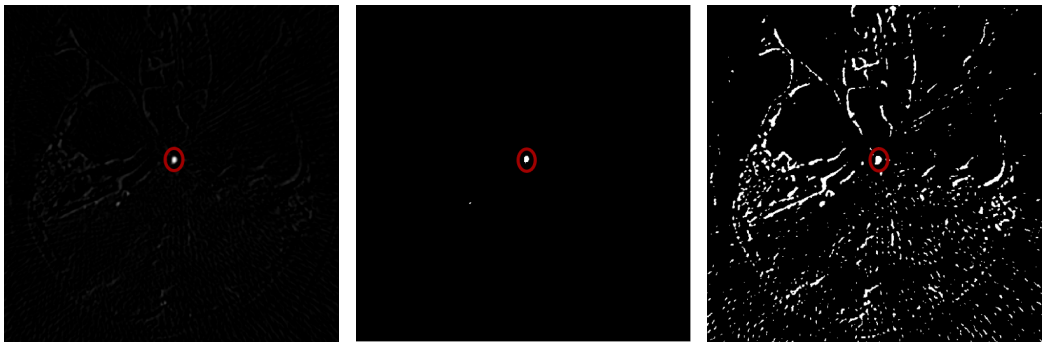

(a) (b) (c)

Figure 2.2: 512 × 512 3D RA CA slice (a) original gray-scale image (b) segmented image using hard-thresholding (c) segmented image using multi-thresholding [lesion is contoured in red]

2. **Edge-based:** These techniques follow the assumption that regions boundaries would experience sharp differences in the intensities. It is inspired by the human perception of objects in real life [62]. Therefore, they partition an image into regions based on abrupt changes in the intensities. These techniques are suitable for images having good contrast [7]. However, they are too noise sensitive compared to threshold-based and

cluster-based techniques. In addition, they do not function well in the following two cases: the presence of too many edges or ill-defined edges [62]. Therefore, edge information is not always reliable.

Edge-based techniques are categorized into two main groups: first derivative methods, which are known also as histogram-based techniques, and second derivative methods, which are known also as gradient-based techniques. The first derivative methods examine the intensity distribution in the neighboring pixels of a certain pixel in order to classify it as an edge or not. These methods are very sensitive to noise and produce thicker edges. Sobel, Prewitt, Roberts, and Canny operators are some examples that fall in the first group. While the second derivative methods detect edges based on the extraction of zero crossing points which indicates the presence of maxima in the image. Laplacian is an example of the second group [9]. Usually, the second category techniques enhance the fine details in an image much better than the first group operators [33]. Figure 2.3 and 2.4 illustrate two segmentation examples of a MRI human skull slice and a 3D RA CA slice using one operator from each group in the edge-based category.

3. **Region-based:** Two techniques are available under this category: region growing and region splitting-and-merging. For the first technique, regions are identified in images based on some predefined criteria as intensity or color. A user selects a seed point for each region, and all the pixels with the same criteria are grouped together to form a homogenous region. The selection of predefined criteria depends on the application and the adopted image modality. For example, intensity levels and spatial properties may be used as regions characterization for gray-scale images [33]. This selection must be done carefully as regions may be merged or

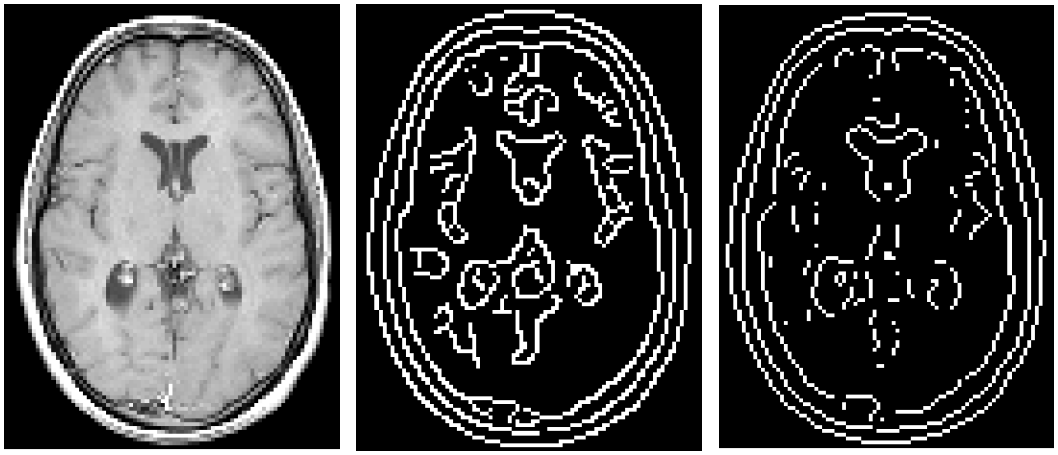

(a) (b) (c)

Figure 2.3: 128 × 128 MRI human skull slice (a) original gray-scale image (b) segmented image using canny edge operator (c) segmented image using Laplacian edge operator

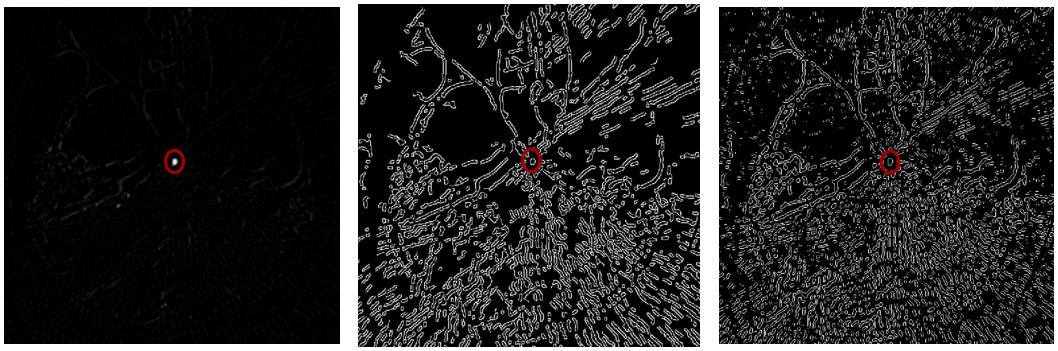

(a) (b) (c)

Figure 2.4: 512 × 512 3D RA CA slice (a) original gray-scale image (b) segmented image using canny edge operator (c) segmented image using Laplacian edge operator [lesion is contoured in red]

spread with adjacent regions [7]. Region growing main limitation is the need for the human interaction to select a seed point and/or to stop the algorithm. However, an automatic selection is possible and addressed in some research works [90, 94]. The accuracy of this technique depends on both seed selection and examination order of pixels or regions.

As for the second technique, split-and-merge regions, no manual seed se-

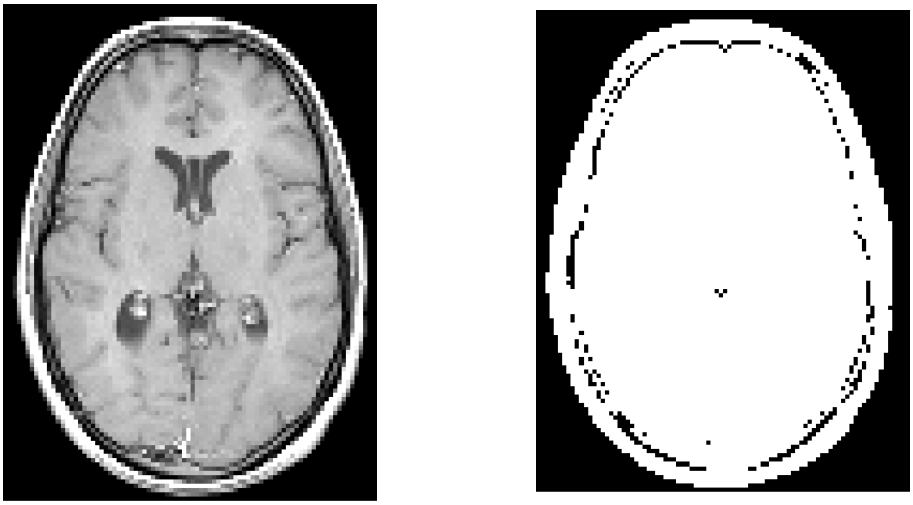

(a) (b)

Figure 2.5: 128 × 128 MRI human skull slice (a) original gray-scale image (b) segmented image using region growing technique

lection is required. Regions are splattered arbitrary and then merged trying to connect related regions. Splitting without merging would result in adjacent regions with identical properties. Therefore, the merging step is crucial to achieving mutual exclusive homogenous regions, which is the main aim of the segmentation [33].

The techniques under this category are useful in delineating a specific anatomical structure or lesion (e.g., tumor) as they divide the image into spatially connected homogeneous regions. They are also less sensitive to noise than threshold-based and edge-based techniques due to the regional properties consideration [7]. Nevertheless, they are expensive in terms of time and memory [62]. In addition, variation in intensities may result in over segmentation or formulation of holes [34]. Figure 2.5 and 2.6 illustrate two segmentation examples of a MRI human skull slice and a 3D RA CA slice using region growing technique.

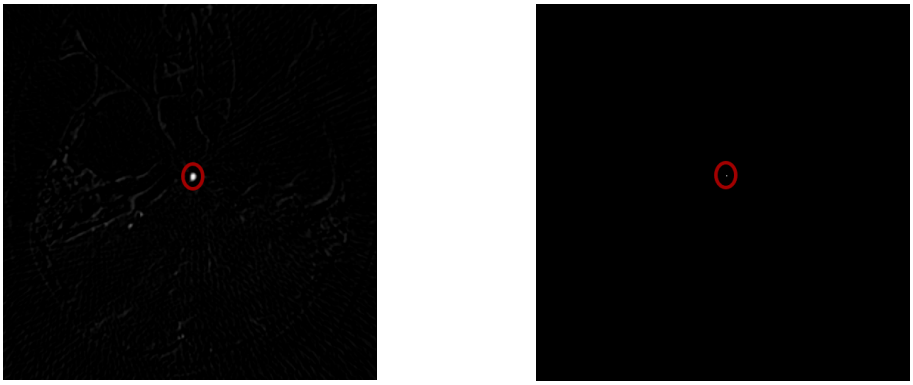

(a) (b)

Figure 2.6: 512 × 512 3D RA CA slice (a) original gray-scale image (b) segmented image using region growing technique [lesion is contoured in red]

4. **Graph-based:** The techniques of this category aim to represent the image as a weighted undirected graph data structure, where pixels are represented as nodes (or vertices). Edges connect these nodes, where non-negative weights are assigned to each one according to some properties to highlight their relationships in an image; some nodes may not be connected if no relationship is found. The segmentation in this category aims to partition the image into regions, where each region is a sub connected graph. Some techniques that fit in this category are: minimum spanning tree [98], shortest path [66], local variation [30], eigenvector [91], random walker [35], dominant set [64, 65], and graph-cut [93, 81, 10] which is the most commonly adopted approach in MIS [3]. These techniques benefit from graph-theory tools [57], where no discretization errors are expected due to the usage of combinatorial operators. Figure 2.7 and 2.8 illustrate two segmentation examples of an MRI human skull slice and a 3D RA CA slice using a graph cut technique, where the image is clustered to foreground and background regions.

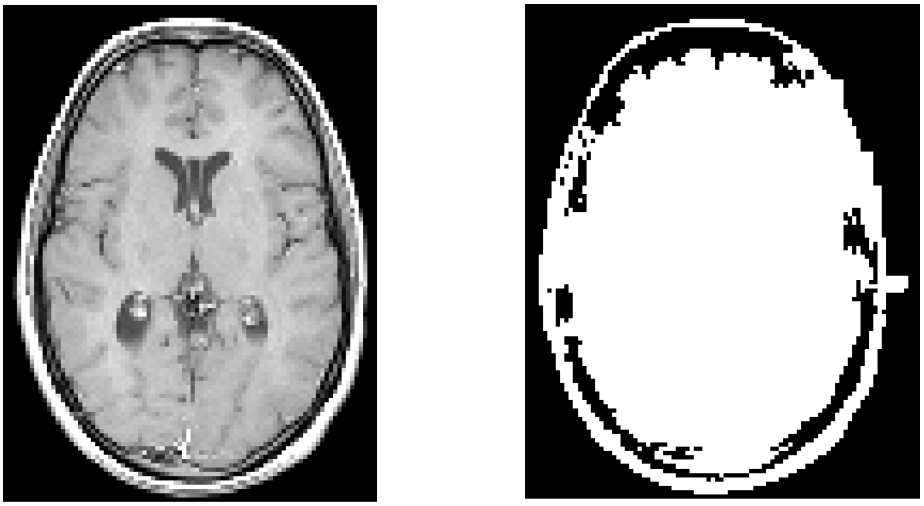

(a) (b)

Figure 2.7: 128 × 128 MRI human skull slice (a) original gray-scale image (b) segmented image using graph cut technique

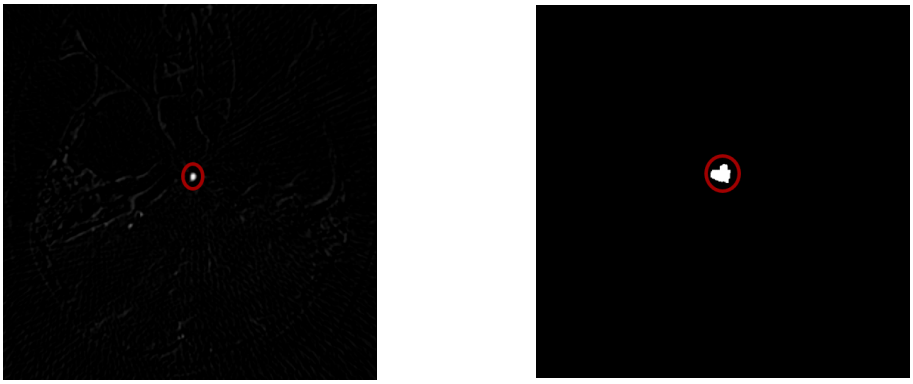

(a) (b)

Figure 2.8: 512 × 512 3D RA CA slice (a) original gray-scale image (b) segmented image using graph cut technique [lesion is contoured in red]

5. **Model-based:** These techniques delineate region boundaries using closed parametric curves, in 2D domain, or surfaces, in 3D domain, that deform under the influence of internal and external forces. The internal forces aim to maintain the internal shapes constraints, as smoothness, during the deformation process. While the external forces are designed

to push or pull the model towards the captured boundaries [41]. These models are built upon a strong mathematical background, where geometry, physics, and approximation theory are combined all together to provide information regarding the location, size, and shape of objects where they integrate high-level knowledge with low-level image processing information [7]. In addition, they can accommodate the variability of anatomical shapes over time. Two main models exist, which are parametric models, known as snakes or explicit techniques, and geometric models, known as level set or implicit techniques.

Models belonging to the first type move explicitly predefined contour points based on energy minimization model. Their main disadvantage is the dependency on the initial curve parametrization placed near to the desired region boundaries aimed to segment. However, these techniques are fast, accurate, and overcome the speckle induced error. Active contours (in 2D domain), active surfaces (in 3D domain), and gradient vector flow are examples of these models. In 2D, the methods are computationally efficient and easy to implement, which is not the case in the 3D domain as the parametrization becomes a harder task [49].

The second type of deformable models come to overcome the limitations of the first type, as the energy here relies on the object' s geometry instead of the curve' s parameters. These models add the time dimensionality to the curve representation. They capture multiple objects, complex boundaries, and handle topological changes. These advantages come with an additional computational cost and lack in terms of accuracy [7]. Geometric active contour, in 2D or Geometric active surfaces, in 3D, are examples of geometric models' techniques. Techniques belonging to this type are used intensively in modern MIS. Figure 2.9 and 2.10 illustrate two segmentation examples of a MRI human skull slice and a 3D RA CA

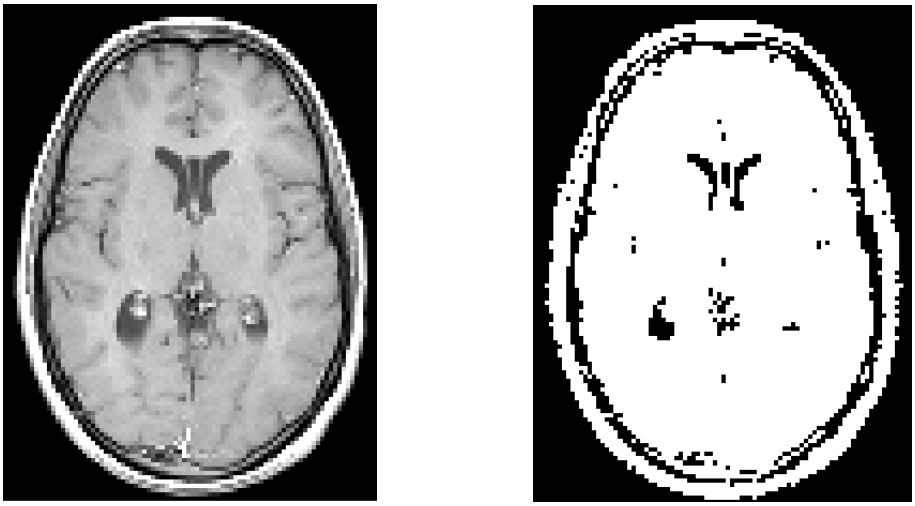

(a) (b)

Figure 2.9: 128×128 MRI human skull slice of (a) original gray-scale image (b) segmented image using active contour technique

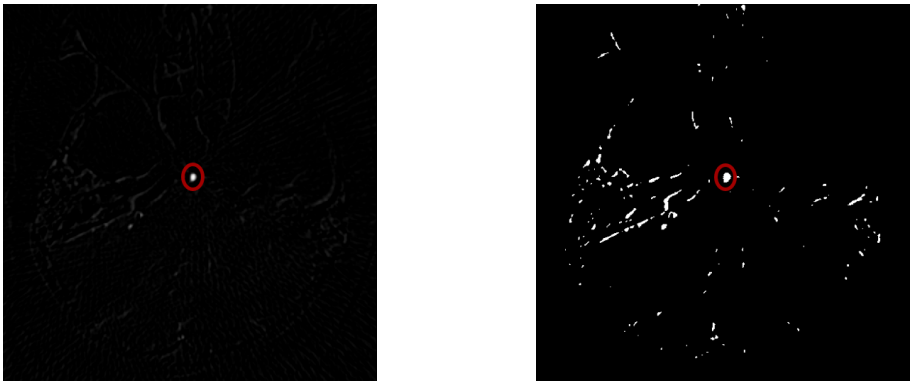

(a) (b)

Figure 2.10: 512×512 3D RA CA slice (a) original gray-scale image (b) segmented image using active contour technique [lesion is contoured in red]

slice using active contour technique, where the image is partitioned into foreground and background regions.

6. **Classification-based:** These techniques are derived from the pattern recognition field and integrated into the image segmentation techniques. They are known as supervised approaches since they partition images

based on already trained/segmented data, where a manual segmentation is carried out in some data to be used as a reference later on in the automatic segmentation. Different classification algorithms, which are known as classifiers, are adopted in MIS as Support Vector Machine (SVM), K-Nearest Neighbors (KNN), Artificial Neural Network (ANN), Naive Bayes (NB), Maximum Likelihood (ML), etc. The main limitation of this category is the need to select and train data; and since MIS can be performed for different modalities and diseases, the training process needs to be considerate again whenever a modality or a disease is changed. Therefore, they are considered as laborious and time-consuming techniques [34].

7. **Clustering-based:** This category is similar to the classification-based techniques but no training data is needed here. This is known also as unsupervised methods. Clustering techniques assume that the number of classes is known in advance, where they group pixels, in 2D domain, or voxels, in 3D domain, with same characteristics into the specified classes trying to maximize the similarity of intra and inter classes. The similarity here is defined by one of the distance measures as the Euclidean or Mahalanobis distance. K-means, Fuzzy C-Means (FCM), and Expectation Maximization (EM) are some examples of these techniques. Their main limitations are: requiring initial initialization, do not incorporate spatial modeling, and their sensitivity to noise. On the other hand, they are computationally fast. These techniques can be used as an initial/coarse segmentation step before applying the sequence of other adopted complementary segmentation techniques. For example, they can be used to generate an initial contour for the deformable models [7]. Figure 2.11 and 2.12 illustrate two segmentation examples of a MRI human skull slice

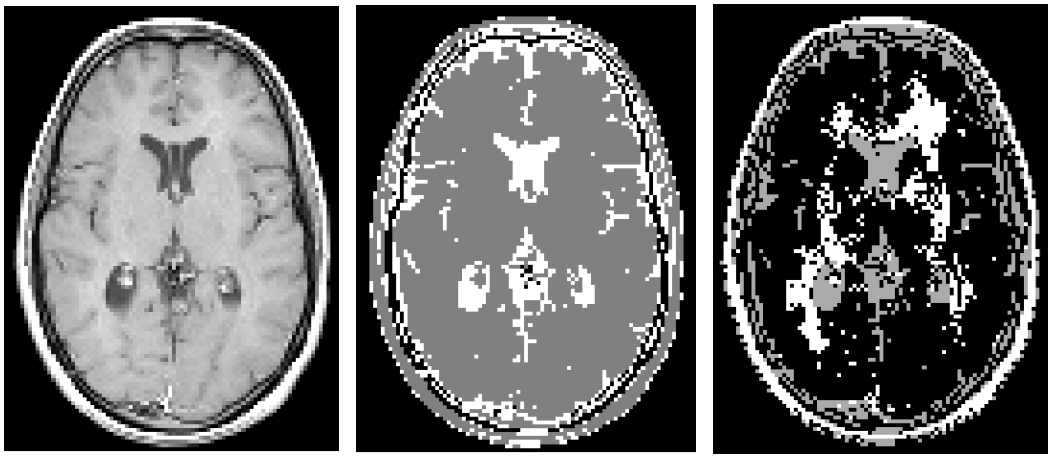

(a) (b) (c)

Figure 2.11: 128 × 128 MRI human skull slice (a) original gray-scale image (b) segmented image using k-means technique (k = 3) (c) segmented image using k-means technique (k = 4)

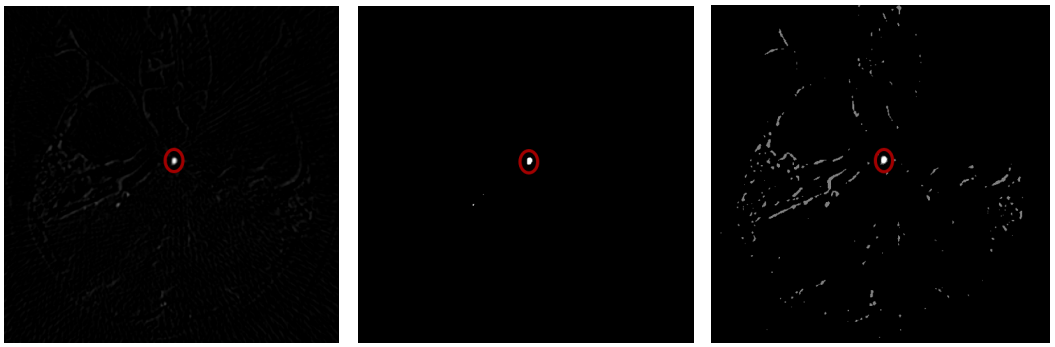

(a) (b) (c)

Figure 2.12: 512 × 512 3D RA CA slice (a) original gray-scale image (b) segmented image using k-means technique (k = 2) (c) segmented image using k-means technique (k = 3) [lesion is contoured in red]

and a 3D RA CA slice using the k-means technique, where the image is partitioned into k regions.

In addition to the segmentation techniques, some pre or post-processing techniques are used along the process to help in producing more accurate and effective segmentation results. Some examples of these techniques are multi-

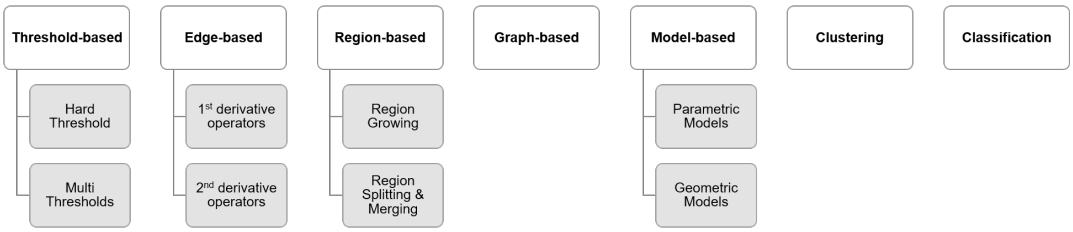

Figure 2.13: MIS Techniques Categorization

modality fusion [44, 56], statistical approaches [50], multiresolution analysis techniques [5, 69], etc.

Multi-modality techniques fuse complementary information of images acquired from different modalities into one image and abandon the superfluous information to obtain a better image representation. As for the statistical approaches, they are used to incorporate prior shape information into the segmentation process. While multiresolution analysis approaches are used to extract hidden or distorted image features using different scales of the same image.

Up to now, no universal technique is available for all type of diseases and/or modalities. For instance, a technique may work effectively for a specific disease and does not work at all for the others or differ in the performance (the accuracy) of the segmentation. Therefore, researchers usually implement algorithms which are optimized for a specific disease, using a specific modality, in a specific domain (2D or 3D domain).

Table 2.1 presents some recent research works about different MIS algorithms available in the literature. For each research work, the following factors are specified: the adopted automation (automatic or semi-automatic algorithm), the used dimensionality (2D or 3D domain), adopted application, the used segmentation techniques without mentioning the pre and post-processing steps, the adopted image modality, and the used performance metrics to evaluate the proposed work quantitatively.

Table 2.1: Overview of some recent MIS techniques in the Literature

Reference	Type	Dimensions	Application	Segmentation Technique	Image Modality	Evaluation
[13]	Semi-automatic	2D	Liver tumor	multi Gabor feature map and non-local active contour	CTA	MOE RDE Execution time
[43]	Automatic	2D	General	PCA and K-means clustering	MRI	PSNR Compression rate Execution time
[51]	Automatic	2D	General	FCM and level set	US CTA MRI	×
[54]	Automatic	2D	Hemorrhages	Mathematical morphology and entropy-based thresholding	Red lesions Fundus images	Sensitivity Specificity
[61]	Semi-automatic	3D	Adjacent hip joint	Edge detection and graph-based minimal path extraction	Radiographic images	RMS ± STD
[70]	Automatic	2D	General	Haralick texture for feature extraction and KNN	CTA	Sensitivity Specificity Accuracy

Continued on next page

Reference	Type	Dimensions	Application	Segmentation Technique	Image Modality	Evaluation
[75]	Automatic	2D	Blood cell	k-means clustering, global threshold, Sobel edge detector, Watershed transform, and mathematical morphology	Microscopic images	Accuracy
[79]	Automatic	3D	Lung cancer	Haar Wavelet Transform (HWT) and ANN	PET	ROC ARE
[82]	Automatic	3D	Multiple sclerosis	Atlas-based approach using topological and statistical atlas	MRI	DSI VD Sensitivity
[90]	Automatic	2D	Liver Diseases	Energy-based region growing	US	TPR FPR FNR

2.2 Cerebral Aneurysm Segmentation

CA segmentation is tackled by many researchers in different ways: in 2D and 3D spatial domain, on different modalities (MRI, CTA, etc.), using automatic or semi-automatic approaches, and using different segmentation techniques. Recently the three main segmentation techniques adopted for developing CA segmentation algorithms are: threshold-based [46, 47, 59, 76, 94], region growing [46, 47, 58, 59, 94], and deformable models [15, 19, 31, 48, 58, 59, 76, 77, 95]; and even though it has been an active research area for a while, the challenge remains in developing a fully automatic approach that is robust, reliable, and reproducible to detect even small aneurysms.

Deformable models' techniques are used extensively in CA segmentation due to their advantages as they are built upon a strong mathematical background where geometry, physics, and approximation theory are combined all together to provide knowledge regarding the location, size, and shape of the objects. These deformable models are combined with other segmentation techniques to end up with the desired results. Firouzian et al. [31] use the Geometric Active Surfaces (GAS) technique, which aims to minimize the energy function. In this context, the energy is composed of three features: intensity, gradient magnitude, and intensity variance. This energy is derived from the manually selected seed point. Moreover, the ROI is also extracted from this seed point. In addition, a prior smoothing is performed using non-linear diffusion to slightly improve their segmentation accuracy. The algorithm is trained using 10 CTA datasets and tested on 5 different CTA datasets. The accuracy of their algorithm is acceptable, where the Dice Similarity Index (DSI) equals to 0.811. However, it has two main limitations. First, the inclusion of the bones in the segmentation of some cases, when an aneurysm is too close to the skull base. Second, the need for a user interaction to select a seed point

within an aneurysm, which exposes the algorithm to intra and inter-operator variability. Sgouritsa et al. [77] select as well the ROI manually as a first step, which includes the CA and some surrounding vascularity. Later, the vessels are segmented using level set method while preserving the topology of the curves and surfaces. Then, the aneurysm is separated from the surrounding parent arteries using s-t minimum graph cut segmentation approach. This developed algorithm is tested on 19 3D DSA datasets. One of its limitation is the heavy dependency on the initialization of the level set function. In addition, the resulted segmentation of the vessels does not guarantee always the anatomy of the touching vessels, which may affect consequently on an CA segmentation. Therefore, this algorithm excludes all datasets where the parent vessels are very close to the CA. In order to evaluate the proposed algorithm, the Average Distance (AD) and the Standard Deviation (STD) of the neck length, dome height, and maximum diameter of an aneurysm are calculated. Chen et al. [15] propose a Lattice Boltzmann Model (LBM) to simulate the Geometric Active Contour (GAC) to take advantage of its high efficiency and parallel processing feature. The algorithm goes through the following steps: Anisotropic diffusion based on LBM is applied first, as a pre-processing step, to reduce the amount of noise in the CTA images. Second, the canny operator is used to detect the edges. Finally, the Lattice Boltzmann Geodesic Active Contour Method (LBGM) is performed. The main purpose of this algorithm is to estimate the volume of both the aneurysm and the thrombus, which it has shown to be effective and overcomes the noise sensitivity existing in the CTA images. However, it is customized to detect mainly giant CAs, where their diameters are larger than 2.5 centimeters. Both Aspect Ratio (AR) and Volume Ratio (VR) are used to evaluate objectively the developed algorithm, where the first one measures the dome neck and the second one measures the thrombus volume. Yang et al. [95] try to abandon the need for the user interaction by using

shape information, as a prior knowledge, to adaptively configure the parameters needed by the GAC method, where the obtained parameters are further refined iteratively. The algorithm is tested on 8 CTA datasets, where the obtained accuracy is perfect for some datasets (DSI = 0.99) and less accurate for others (DSI = 0.86). Sen et al. [76] propose a threshold-based level set method. They combine both models: GAC and Chan-Vese to integrate boundary and regional information. The latter model, Chan-Vese, is used first to calculate the appropriate threshold value. Later, this value is updated iteratively during the segmentation process. The proposed method could be processed in two modes: full-automatic or semi-automatic, depending on the shape complexity of the aneurysm. In the semi-automatic approach, the seed point for the GAC method is selected manually; as for the full-automatic approach, the threshold value and gradient magnitude parameters are used to form the speed function automatically which affect directly the quality of the segmentation. The algorithm is tested on 8 3D CTA datasets, where 6 performance metrics are calculated to evaluate the developed algorithm, which are Volume Difference (VD), Jaccard's Measure (JM), False Positive Ratio (FPR), False Negative Ratio (FNR), Hausdorff Distance (HD), and Mean Absolute Surface Distance (MASD). As for Nikravanshalmani et al. [59], they combine both region growing and level set techniques. The first technique, region growing, is used to extract the cerebral arteries where the needed seed point is selected automatically based on both the slice entropy and the prior anatomical knowledge. As for the second technique, which is the level set method, it segments an aneurysm by separating it from the parent vessels. This algorithm also requires manual interaction to initialize the level set technique. The same authors improved their algorithm in [58] by adding a 3D conditional morphology technique but still, a manual interaction is needed. The improved algorithm goes through five steps. First, region growing technique is used to segment cerebral arteries. Later,

a seed point is selected manually within the aneurysm area. Next, a coarse segmentation is obtained by applying a conditional morphological operation. Then, an edge-based level set technique is implemented to get an exact and fine segmentation of the aneurysm. Finally, a conditional morphological operation is applied again to separate the aneurysm from the parent arteries. The proposed algorithm is implemented mainly to detect saccular aneurysms, which has specific aneurysmal shape. In both works [59, 58], 15 3D CTA datasets are used to test the algorithms, where only a subjective evaluation is carried out. Dakua et al. [19] combine the level set technique with a Multiscale Principle Component Analysis (MS-PCA). The multiscale feature is implemented here using the Gaussian pyramid to handle the variation of the vessels' width. The algorithm is performed on the manually selected ROI, where an aneurysm is suspected to appear. The values of the free parameters in the algorithm are determined by training 7 Phase Contrast Magnetic Resonance Angiography (PC-MRA) datasets. These parameters greatly impact the segmentation accuracy and selecting only 7 datasets may not be enough to guarantee the algorithm' s reliability to adopt it in the clinics. Law and Chung [48] use an intensity-based algorithm in conjunction with the level set technique. Their approach tries to handle the intensity variation of the vascularity and the low contrast of the aneurysmal region(s). Therefore, they have used two types of descriptors: boundary and regional ones. The first descriptor uses a multi-range filter to handle the size variation of the vascularity. As for the second descriptor, it reduces the effect of noise, suppresses the responses induced from the high-intensity vessels, and avoids missing low-intensity aneurysms. The algorithm is tested on a phantom volume and 4 PC-MRA datasets, where a good accuracy is achieved (DSI = 0.8).

So far, all the above-discussed algorithms use the deformable models as one of its methods to segment the CA. However, there are some other algorithms in

the literature where deformable models are not considered in their implementation. Yang et al. [94] develop an algorithm using global threshold and region growing techniques, where the values needed by both techniques (the threshold and the seed point values) are selected automatically. These techniques are used to segment the intracranial vessels and locate the Points of Interest (POIs), which represent the aneurysm candidates. Later, the algorithm goes on to collect more POIs and keep only the suspected aneurysms based on some features calculations. The proposed approach is tested on 92 3D Time-of-Flight Magnetic Resonance Angiography (TOF-MRA) datasets, where the ones containing already treated aneurysms (e.g., clipped or coiled CAs) are not considered, as they need more accurate detection rate. The results of the developed algorithm vary too much depending on the selected operating point and the size of the CA. As for both works proposed by Lauric et al. [47, 46], they segment vascular vessels through thresholding and region growing. The authors introduce for the first time the usage of the writhe number in CA segmentation on 3D RA datasets. In [46], the writhe number is used to detect the aneurysms, where non-tubular segmented regions are identified as aneurysms. The main limitation of this algorithm is its reliance on having high-resolution images. Therefore, there is a direct relationship between the accuracy of the proposed segmentation algorithm and the modality used to acquire images. As in [47], the authors go deeper and try to distinguish between ruptured and unruptured aneurysms using geometric characteristics, where the writhe number is used here to interpret these geometrical characteristics.

Almost all of the above-presented research works require a manual interaction from a user to initialize some certain parameters. This interactivity is laborious, prone to inter and intra operator variability, and depends heavily on the experience of the operators which affects directly the final segmentation accuracy. However, when comparing the performance of full automatic algorithms

with semi-automatic ones, the latter group wins the battle; as in automatic approaches, the accuracy varies considerably across different datasets. For example, in [95], the accuracy ranges from $[86.1\% - 99.2\%]$ for 8 datasets. As in [94], the accuracy also varies, where the sensitivity ranges from $[80\% - 95\%]$ for CAs larger than 5 millimeters (mm) and from $[71\% - 91\%]$ otherwise. While in [76], the algorithm can only operate automatically if the images are not very complex; otherwise, a semi-automatic path is taking over to reduce the complexity of the task. To summarize, there is a trade-off between semi-automatic and full-automatic approaches. The methods of the first category are easier to implement and offer consistent accuracy; while the methods of the second category offer reproducibility and reduce both the computational time and the number of the needed labors since no interaction is required. Therefore, the main challenge for the researchers, in the time being, is to implement a robust and reliable full-automatic approach to segment CA regardless of its shape, location, and size which is our target in this thesis. Table 2.2 summarizes all the above-discussed CA segmentation algorithms, which represent the recent state-of-the-art research works in this field.

Table 2.2: Overview of some recent CA segmentation algorithms in the Literature

References	Type	Dimension	Segmentation Techniques	Image Modality	Evaluation	
					Subjective	Objective
[15]	Semi-automatic	2D	LBM based on anisotropy diffusion, canny operator, and LBGM method	CTA	✓	AR = 3.36 VR = 62.13%
[19]	Semi-automatic	2D	MS-PCA and level set technique	PC-MRA	✓	FPR = 1.9% FNR = 0.75% Specificity = 75% HD = 2.79mm
[31]	Semi-automatic	3D	GAS with energy minimization	CTA	×	DSI = 81.1% ASD = 0.162mm VD = 12.12mm^3
[38]	Automatic Semi-automatic	3D	Multiscale sphere-enhancing filter and Linear discriminant function	CE-MRA TOF-MRA CTA	×	Sensitivity = 95% FPR = [8.2% − 22.8%]
[46]	Semi-automatic	3D	Threshold, region growing, and writhe number	RA CTA	×	FPR = [0.66% − 5.36%] Sensitivity ≃ 100%
[47]	Semi-automatic	3D	Threshold, region growing,	RA	×	Accuracy =

Continued on next page

References	Type	Dimension	Segmentation Techniques	Image Modality	Evaluation	
					Subjective	Objective
			and writhe number			$[71 \pm 3\% - 86 \pm 2\%]$
[48]	Semi-automatic	3D	Intensity-based approach	PC-MRA	×	DSI = 80.04%
			with the level set technique			Sensitivity = 83.65%
						Specificity = 99.86%
[58]	Semi-automatic	3D	Region growing, edge-based level set,	CTA	✓	×
			and conditional morphology			
[59]	Semi-automatic	3D	Region growing and level set technique	CTA	✓	×
[77]	Semi-automatic	3D	Topology preserving Level set	DSA	×	STD
			and graph cut techniques			AD
[76]	Semi-automatic	3D	Threshold-Based Level Set method	CTA	×	VD = 2.51%
	Automatic					JM = 91.59%
						FPR = 3.31%
						FNR = 3.48%
						HD = 0.89 pixel
						MASD = 0.08 pixel
[94]	Automatic	3D	Thresholding, region growing	TOF-MRA	×	Sensitivity = [80% − 95%]
			and dot enhancement filter			(CA $\geq$ 5 mm)

Continued on next page

References	Type	Dimension	Segmentation Techniques	Image Modality	Evaluation	
					Subjective	Objective
[95]	Automatic	3D	Adaptively-configured geometry active contour	CTA	×	Sensitivity = [71% − 91%] (CA ≤ 5 mm) DSI = [86.1% − 99.2%]

2.3 Multiresolution and Statistical Approaches for Medical Image Segmentation

Multiresolution analysis techniques are introduced to overcome the shortage of the segmentation process. As the latter one assumes that image features, which are mainly the image contours, are already apparent; and it attempts only to allocate image pixels into partitions according to these apparent features using some segmentation techniques. However, due to the introduced artifacts by the acquisition methods/scanners, these features are usually hidden or distorted. Therefore, multiresolution analysis techniques come to empower the segmentation algorithm by extracting features that cannot be easily extracted from the normal image resolution/scale. The main motivation to adopt multiresolution analysis techniques is the presence of low and high contrast objects simultaneously in the image [33]. Their main advantages are the high resistance to noise and high processing speed. In addition, they are built upon solid mathematical basis [72]. Different techniques are used to implement the multiresolution analysis concept such as Wavelet, Ridgelet, Curvelet, and Contourlet transforms. These techniques have been already embraced in the MIS [5, 69].

As for the **statistical approaches**, they incorporate prior shape information into the segmentation process, which increases dramatically the performance. Some of these approaches are: Principle Component Analysis (PCA), Maximum a Posterior (MAP), Finite Mixture (FM) model, and Markov Random Field (MRF). These approaches build models based on the distributions of an image data and try to segment it by minimizing a defined cost function using a set of mathematical equations that describes the behavior of an object of study. This cost function is associated with each pixel in order to measure the "cost" of giving a certain label to a certain pixel.

The two above introduced techniques, multiresolution and statistical approaches, help in developing more accurate segmentation algorithms. In the literature, different works are proposed based on these two approaches to segment medical images [4, 6].

CT, which is a multiresolution analysis technique, and HMRF, which is a statistical approach, are both surveyed in the literature in Section 2.3.1 and 2.3.2 respectively as they are the main adopted techniques in the proposed CA segmentation algorithm.

2.3.1 Contourlet Transform

In the literature, CT is adopted for different medical images applications as denoising [40, 42, 74], multimodality fusion [20, 56], compression [37], watermarking scheme [27], and segmentation [52, 53, 55]. The general process for all of these applications goes as follow: The medical image is decomposed using CT. Then, the obtained coefficients are handled differently. Finally, the inverse CT is applied to reconstruct the medical image. So, the main difference takes place during the second step to realize the desired application aim.

In MIS, CT is used jointly with different techniques to segment medical images in recent years. Moayedi et al. [55] try to automate the mass classification problem of mammograms. Their proposed algorithm starts first by segmenting the ROI. Later, CT is used for feature extraction. Next, the genetic algorithm is applied for feature selection. Finally, different classifiers are used to classify breast abnormalities. Liu et al. [53] decompose the image using CT. Then, a watershed algorithm is applied on the coefficients. Next, an edge detection method is applied. Finally, the image is reconstructed using the inverse contourlet. Li and Li [52] decompose the image using the contourlet transform. Next, the M-most significant coefficients are kept as they are, and the remaining coefficients are set to zero. Later, a c-means clustering algorithm is

Table 2.3: Overview of some recent uses of CT for MIS in the literature

Reference	Disease	Segmentation Techniques	Image Modality	Evaluation	
				Subjective	Objective
[52]	General	CT with c-means clustering	CTA	✓	×
[53]	General	CT with watershed algorithm and edge detection	CTA	×	Execution time
[55]	Mass Classification	CT with genetic algorithm and classifiers	Mammograms	×	Sensitivity Accuracy Specificity

applied, where the coefficients are clustered into two categories. Finally, the image is reconstructed. Table 2.3 summarizes all the above-discussed examples/applications.

2.3.2 Hidden Markov Random Field

Medical images consist of homogenous regions as the anatomical structures consist most probably of more than one pixel. Hence, the neighboring pixels have similar properties as the intensity, texture, color, etc. This characteristic encourages the adoption of the HMRF model as it is designed to capture these spatial contextual constraints, where the correlated neighboring pixels are categorized into the same partition/region.

HMRF model is a statistical approach, in the stochastic domain, used along with the segmentation techniques introduced in section 2.1. This model provides prior knowledge which simplifies greatly the MIS process. It is a special case of Hidden Markov Model (HMM), as it is generated by MRF instead of Markov chain to handle 2D and 3D problems, since models derived from Markov chains are designed for 1D problems [100].

HMRF model is used for different applications as image labeling [14], speech recognition [83], handwriting recognition [29], gesture recognition [96], etc.

In MIS, HMRF is adopted differently in recent years. Abdulbaqi et al. [2] used the HMRF-EM to diagnose brain tumor in CTA scans. They have first applied

a canny operator to detect edges. Later, a Gaussian blur filter is applied to smooth the performance. Next, a k-means clustering is applied to initialize the segmentation and parameters. Then, the final segmentation and parameters are obtained from HMRF-EM framework which maximizes the expected likelihood function by iterating through the E-Step and E-Step. Finally, a hard threshold is applied to obtain the final tumor region. As for Patra and Pradhan [63], they incorporate the HMRF model into the Fuzzy Clustering Expectation Maximization (FCEM) segmentation algorithm to develop an unsupervised framework, where the image class labels are estimated by maximizing the fuzzy membership function. Here, the unknown model parameters, number of classes, and the image labels are initialized randomly/arbitrary without affecting the final results. Zhang et al. [99] propose to incorporate the Clonal Selection Algorithm (CSA) and Markov Chain Monte Carlo (MCMC) into the HMRF model to segment kidney and liver in MRI images. This combination overcomes the limitation of traditional HMRF-based segmentation approach as the optimization is done globally instead of locally. On the other hand, the proposed approach is computationally high. In addition, the MCMC requires a large number of simulation draw and the CSA requires many parameters estimation which questions its applicability to all cases. The proposed algorithm goes through three iterative steps. First, class labels are estimated using MCMC technique. Second, a bias field correction is employed. Third, the statistical parameters are estimated using the CSA algorithm. Said and Azaiz [73] adopt the HMRF-EM framework as well to segment the liver tumor from CTA images, but instead of adopting the normal version of EM, a Bootstrap version is applied to enhance the computational complexity, where the segmentation is applied on a sample instead of the entire image. A post-processing step is required to refine the segmentation using morphological adjustment and active contours. The accuracy of the proposed algorithm decreases in the following

Table 2.4: Overview of some recent uses of HMRF model for MIS in the literature

Reference	Disease	Segmentation Techniques	Image Modality	Evaluation	
			Modality	Subjective	Objective
[2]	Brain tumor	HMRF with EM, k-means, canny edge, and hard-thresholding	CTA	×	VD Accuracy
[63]	kidney and liver tumor	HMRF with FCEM	×	✓	MCE VD
[73]	Liver tumor	HMRF with EM	CTA	×	VD RAVD
[73]	Liver tumor	HMRF with EM	CTA	×	VD RAVD
[99]	Brain liver	HMRF with CSA and MCMC	MRI	×	DSI VD

two cases: First, if the tumor density value approaches the hepatic tissue density value. Second, if the tumor is close to the liver boundaries of the liver, where its density value would be the same as the adjacent organs density value. Table 2.4 summarizes all the above-discussed research works.

2.4 Summary

The presented material in this chapter explores the main concepts of this thesis in the literature starting first by the MIS; later some state-of-the-art CA segmentation algorithms are investigated; and finally, the two main adopted techniques, which are based on multiresolution and statistical approaches, are studied in the MIS field.

In this work, HMRF model, which is a statistical approach, in conjunction with CT, which is a multiresolution analysis technique, is used to model medical image pixels in the contourlet domain to get better statistical information in order to achieve a robust and accurate CA segmentation. In the next chapter, the proposed CA segmentation algorithm is presented and explored in details.

Chapter 3: Methodology

This chapter presents the proposed Cerebral Aneurysm (CA) segmentation algorithm. Section 3.1 provides an overview of the general algorithm workflow. Section 3.2 deals with the mathematical background of the two main adopted techniques. Later, Section 3.3 discusses the details of the proposed algorithm.

3.1 Overview

The proposed CA segmentation approach consists mainly of two promising methods, implemented in a Two-Dimensional (2D) domain. The first method is the Contourlet Transform (CT), developed by Do and Vetterli [24]. As for the second technique, it is the Hidden Markov Random Field model with Expectation Maximization algorithm (HMRF-EM), introduced by Zhang et al. [100] for brain MRI segmentation. Figure 3.1 depicts the complete flowchart of the proposed CA segmentation algorithm.

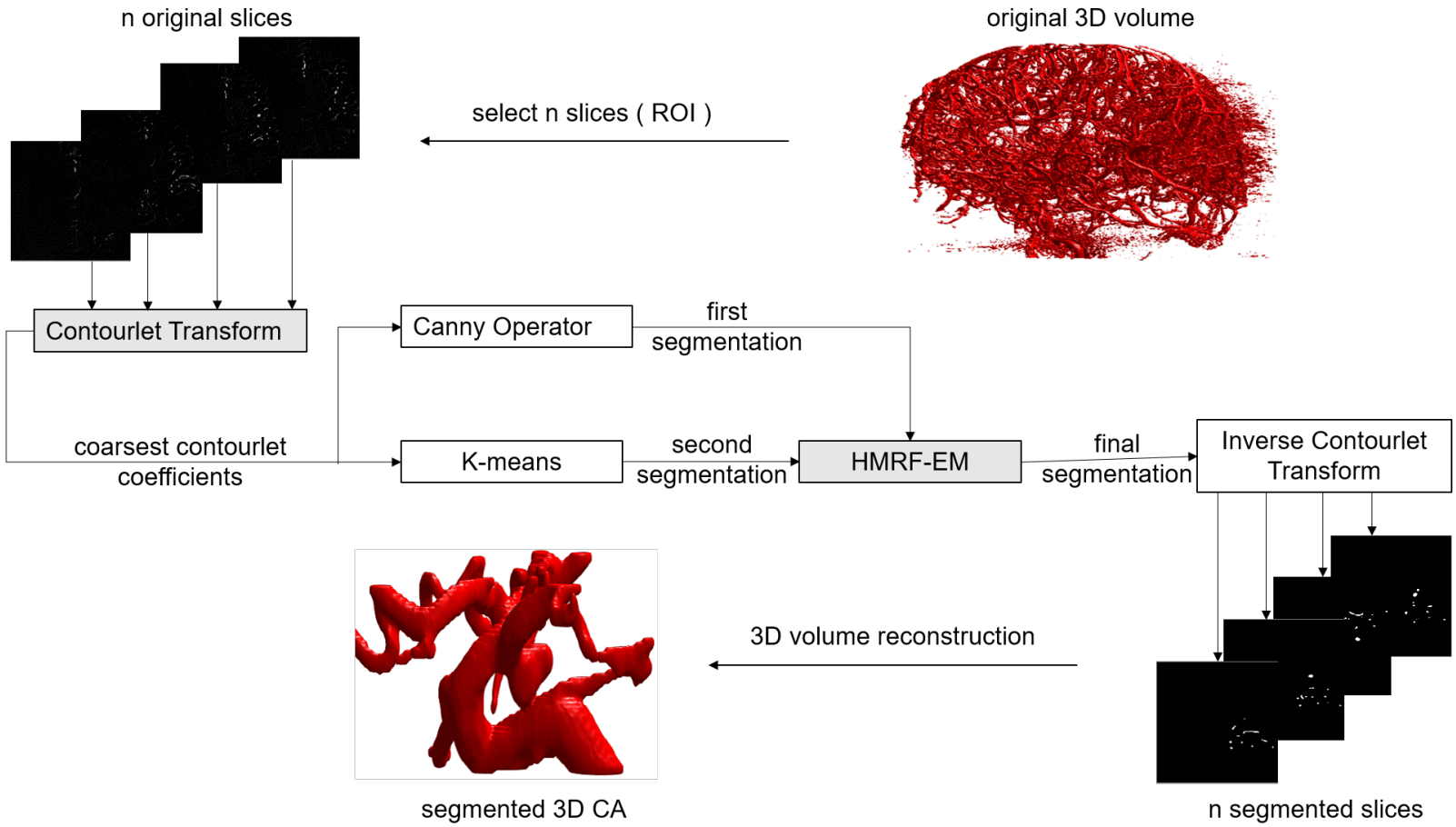

Figure 3.1: Flowchart of the proposed segmentation

3.2 Mathematical Background

In this section, the mathematical background of the two main adopted techniques in the proposed CA segmentation algorithm are introduced in the following sub-sections 3.2.1 and 3.2.2.

3.2.1 Contourlet Transform

CT is a new true 2D transform [69]. It realizes the identified wish list of Do and Vetterli in the discrete domain, which includes the following properties [25, 26]:

- **Multiresolution:** The ability to decompose an image, from coarse to fine, into successively approximated scales/resolutions.
- **Localization:** The basis elements, which are image pixels, should be localized in both spatial and frequency domains.
- **Critical sampling:** The basis or frame representation should be formulated with a small redundancy.
- **Directionality:** The ability to apply different number of directions for each different resolution, where the number of directions is much more than the ones offered by the separable wavelets.
- **Anisotropy:** A variety of elongated shapes with different aspect ratio should be used to represent the basis elements in order to capture the smooth contours in an image.

In addition, this transformation provides a sparse representation which saves a significant amount of memory and offers a simple and fast data processing. This sparsity is obtained by applying first the multiresolution decomposition function, followed by a local directional transform to gather the nearby basis functions at the same resolution into linear structures. The decoupling of the

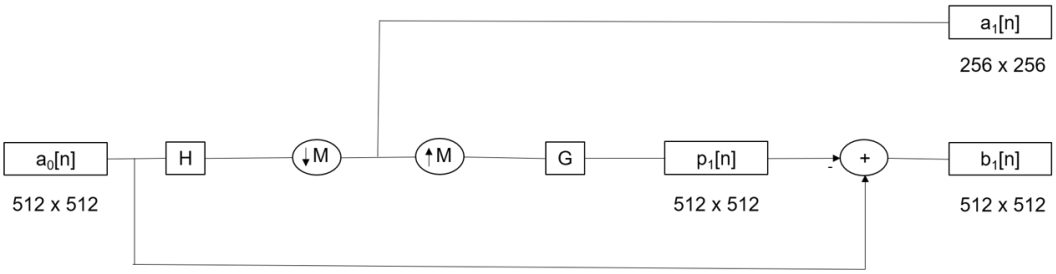

Figure 3.2: LP process for one level of decomposition

multiresolution and directional decomposition stages offers a simple and flexible transform but at a cost of a small redundancy (up to 33%).

All the aforementioned CT properties are achieved by adopting the Pyramidal Directional Filter Bank (PDFB) proposed by Do and Vetterli [23]. This double filter bank combines Laplacian Pyramid (LP) and Directional Filter Bank (DFB) to extract the fine desirable features.

Laplacian Pyramid

LP, introduced by Burt and Adelson [12], allows the multiresolution representation of an image $a_0[n]$ to capture points singularities (edges) by removing the noise. This representation is obtained by going through the following process: First, derive a coarse approximated image $a_1[n]$ by applying a lowpass filter (H) and down-sampling ($\downarrow M$). Second, derive a predicted image $p_1[n]$ from $a_1[n]$ by applying on it a highpass filter (G) and upsampling ($\uparrow M$). Third, derive a fine detailed image $b_1[n]$ by calculating the difference between the original image $a_0[n]$ and the predicted image $p_1[n]$. The downsampling, as mentioned before, is only applied to the lowpass channel, which ensures that images would never have scrambled frequencies. This process can be iterated to get more resolution representations by repeating the same workflow on the coarse image $a_1[n]$ [26]. Figure 3.2 illustrates this process clearly for one level of decomposition.

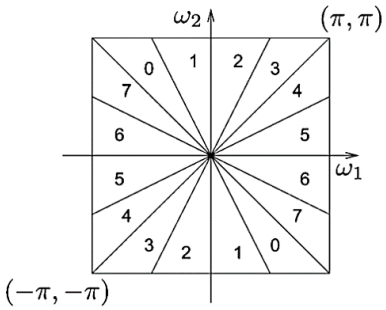

Figure 3.3: DFB decomposition, where $l = 3$ and there are $2^l(2^3 = 8)$ wedge shaped frequency bands [26].

Directional Filter Bank

DFB, introduced by Bamberger and Smith [8], decomposes an image into multiple directions to capture high-frequency content, as smooth contours segments and directional edges, by formulating the captured point singularity into a linear structure. DFB is implemented via an l-level binary tree decomposition that leads to wedge-shaped frequency partitions of 2^l subbands. This implementation is derived by the following process: First, apply two-channel quincunx filter bank fan filters [87] to partition a 2D spectrum into two directions: horizontal and vertical. Second, apply a shearing operator to reorder the image samples. The key idea in DFB is to select the appropriate combination of quincunx filter banks, at each node of the binary tree, and the shearing operator to end up with the desirable 2D spectrum division. Figure 3.3, adapted from [26], illustrates an example of applying DFB on an image.

Contourlet Transform Process

After introducing LP and DFB separately, this section presents their combination that formulates the PDFB, which realizes the CT properties. The general process of the contourlet works as follow: First, the image $a_0[n]$ is passed to the LP filter to produce two images as an output: a coarse/approximated/lowpass

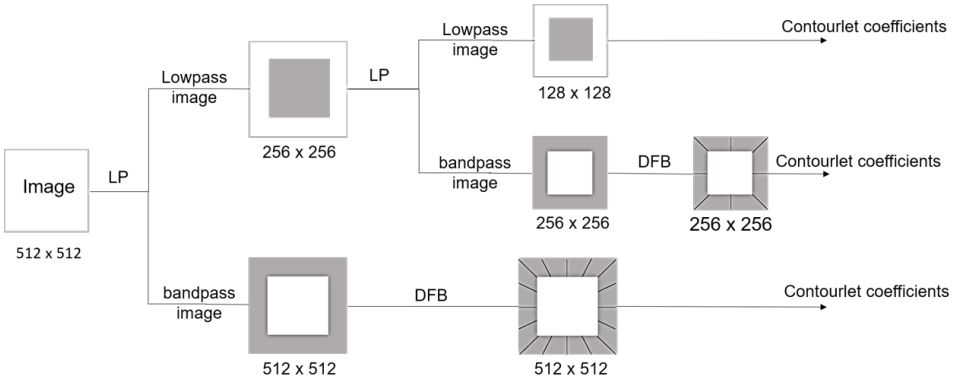

Figure 3.4: CT process for 512 × 512 image, where L_j=2 and $k = (8, 4)$ respectively for each level

image $a_1[n]$ and a fine/detailed/bandpass image $b_1[n]$. The latter image, the bandpass one, is passed to the DFB to produce 2^{L_j} bandpass directional images $c_{j,k}^{L_j}[n]$. As for the first image, the lowpass image, it is passed again to the LP to repeat the same process again until a certain predefined number of decomposition levels L_j is reached. The final output of the CT is a lowpass subband $a_j[n]$ and several bandpass directional subbands $c_{j,k}^{L_j}[n]$, which are called as the contourlet coefficients. Figure 3.4 illustrates the CT process to decompose a 512 × 512 image into two levels, where 8 and 4 directions are applied at each level respectively.

CT has different advantages defined hereafter: It has the adeptness at capturing geometrical smoothness of 2D contours and anisotropy in the discrete domain. In addition, it has a high degree of directionality as it allows to define different directions for different scales, which is not possible in other multiresolution analysis techniques. In terms of complexity, it requires O(N) operations for an image with N-pixels [69]. To summarize, the CT takes a 2D image $a_0[n]$ as an input and decomposes it into coefficients $\left\{a_j[n], c_{j,k}^{L_j}[n]\right\}$ which can be expressed mathematically by the equations 3.1 and 3.2 respectively.

Algorithm 1 Contourlet Transform Algorithm

$L_j \leftarrow$ initialize the number of decomposition level
K $\leftarrow$ initialize the number of directions for each L_j
$img \leftarrow$ initialize the input image $a_0[n]$
for $j \in \{1, ..., L_j\}$ **do**
  $[a_j[n],\ b_j[n]] \leftarrow$ apply LP decomposition on img
  for $k \in \{1, ..., K_{L_j}\}$ **do**
    $c_{j,k}^{L_j}[n] \leftarrow$ apply DFB decomposition on $b_j[n]$
  end for
  $img \leftarrow$ initialize $a_j[n]$ as the new image to decompose
end for
return $a_j[n],\ c_{j,k}^{L_j}[n]$

$$a_j[n] = f, \theta_{j,k,n}^{(L)} \longrightarrow \theta_{j,k,n}^{(L)} = \sum_{n \in Z^d} g_k[n] \phi_{j,k}(t) \tag{3.1}$$

$$c_{j,k}^{L_j}[n] = f, \rho_{j,k,n}^{(L)} \longrightarrow \rho_{j,k,n}^{(L)} = \sum_{n \in Z^d} g_k[n] \varphi_{j,n}(t) \tag{3.2}$$

, where $\theta_{j,k,n}^{(L)}$ is LP basis function for scale decomposition and $\rho_{j,k,n}^{(L)}$ is DFB basis function for directional decomposition. The parameters j, k, d, and n, used in the equations 3.1 and 3.2, are defined respectively: number of levels/scales, number of directions for each level, dimensionality (in our case it is equal to 2 since we are working in the 2D domain), and a scale parameter along the frequency axis. [22, 25, 26] provide more detailed mathematical analysis of these above illustrated equations. The CT pseudocode is provided in Algorithm 1.

3.2.2 Hidden Markov Model with Expectation Maximization

HMRF model tries to segment the medical images based on the spatial correlation between neighboring pixels using two sets of random variables. Some important notions about this model are:

- **Random field:** It is a family of random variables, in which they can take on different values randomly; in this context, the random variables are the intensity levels in an image (i.e., in an 8-bit gray-scale image the random variables can range from 0 to 255); and based on the Markov probability, the probability of each random variable depends on its neighborhood rather than all the remaining variables. In the HMRF model, two random fields exist:

  - **Hidden random field:** $X = \{x = (x_1, x_2, .., x_N) \mid x_i \in L, i \in S\}$ is a random field in a finite state space L and indexed by a set S with respect to a neighboring system of size N.

    The state of this field X is unobservable/hidden; and every x_i is independent of all other x_j.

  - **Observable random field:** $Y = \{y = (y_1, y_2, .., y_N) | y_i \in D, i \in S\}$ is a random field in a finite space D and indexed by a set S with respect to a neighboring system of size N.

    The random field Y is observable and it can only be defined with respect to X, where y_i follows a conditional probability distribution given any particular configuration of $x_i = l$: $p(y_i|l) = \{f(y_i; \theta_l),\ \forall l \in L\}$, where θ_l is the set of the involved parameters.

- **Parameters:** The set of involved parameters, θ_l, are unknown. Therefore, a model fitting is adopted to estimate them. In our context, the parameters are mainly the mean and the standard deviation $\{\mu, \sigma\}$.

- **Conditional independence:** The two random fields (X, Y) are conditionally independent

  $P(y|x) = \prod_{i \in S} P(y_i, x_i) = P(y|x)\ P(x) = P(x)\ \prod_{i \in S} P(y_i, x_i)$

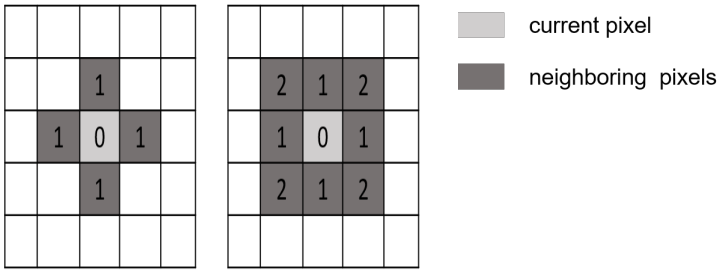

Figure 3.5: Different neighboring system in HMRF model (a) 1^{st} order neighboring system (N = 4) (b) 2^{nd} order neighboring system (N = 8)

- **Clique:** It is a subset of pixels, where every pair of distinct pixels are neighbors. A value is assigned to each clique (c) in order to define the clique potential $V_c(x)$, where the sum of all of these values results in the energy function, $U(x)$, that we aim to minimize it.

$$U(x) = \sum_{c \in C} V_c(x) \tag{3.3}$$

- **Neighborhood system:** It is a way to define some surrounding pixels for a specific pixel, which reflects how far the contextual constraint is [14]. The two commonly used systems are: the first order and the second order neighboring systems, where four and eight neighbors are defined respectively for each pixel. Figure 3.5 depicts these two systems. Therefore, for any pair (x_i, y_i), given the neighboring configuration x_N of x_i, their joint probability is $P(y_i, x_i|x_N) = P(y_i|x_i)\ P(x_i|x_N)$

As any model, HMRF model can only be complete when all of its parameters, θ_l, are known. Therefore, different algorithms are incorporated to fit this model and solve the incomplete data, class labels and parameters. Some examples of these algorithms are: Clonal Selection Algorithm (CSA) [99], Gaussian Mixture

Model (GMM) [89], Fuzzy C-Means (FCM) [16], and Expectation Maximization (EM) [2, 100]. The latter approach is the one selected and adopted in this work.

The HMRF-EM framework, which is first introduced by Zhang et al. [100], incorporates the EM algorithm with the HMRF model not only to estimate the parameters but also to segment the medical images using iterative updates. The framework starts first by initializing both: the segmentation and parameters (means μ and standard deviations σ). Then, iteratively, it goes through the Expectation Step (E-Step) and Maximization Step (M-Step) to update these parameters and the initial segmentation until no development is observed or until a certain pre-fixed number of iterations is reached.

The **E-Step** updates the segmentation by assigning to each pixel an estimated class label $\hat{x}$ from a set of labels L. The assignment is done based on the MAP criterion which tries to minimize the posterior energy using the current parameters estimate; during the energy maximization the conditional posterior probability distribution $P(Y|X)$ gets maximized. Equation 3.4 illustrates the formula for the energy calculation.

$$\hat{x} = \arg\min(\, U(y|x) + U(x)\,) \tag{3.4}$$

, where $U(x)$ is the energy function illustrated above in the equation 3.3 and $U(y|x)$ is the likelihood energy illustrated below in the equations 3.5.

$$U(y|x) = \sum_{i \in S} [\, \frac{(y_i - \mu_{x_i})^2}{2\sigma^2} + \log(\sigma_{x_i})\,] \tag{3.5}$$

While the **M-Step** updates the parameters based on the ML criterion, which tries to maximize the expected likelihood found in the E-Step. The formula 3.6

Algorithm 2 HMRF-EM Algorithm

$[\theta^{(0)},\hat{x}^{(0)}] \leftarrow$ initialize the parameters and segmentation
$EM\_itr \leftarrow$ initialize the number of EM iterations
$MAP\_itr \leftarrow$ initialize the number of MAP iterations
for $i \in \{1, ..., EM\_itr\}$ **do**
  for $j \in \{1, ..., MAP\_itr\}$ **do**
    $\hat{x}^{(j)} \leftarrow$ Update the segmentation $\hat{x}^{(j-1)}$ based on the MAP criterion
  end for
  $\theta^{(i)} \leftarrow$ Update the parameters $\theta^{(i-1)}$ based on the ML criterion
end for
return $\theta^{(EM\_itr)}, \hat{x}^{(MAP\_itr)}$

and 3.7 illustrate the equations to calculate the parameters μ and σ respectively.

$$\mu = \frac{\sum_{i \in S} P^{(l)}(l|y_i) y_i}{\sum_{i \in S} P^{(l)}(l|y_i)} \tag{3.6}$$

$$\sigma = \sqrt{\frac{\sum_{i \in S} P^{(l)}(l|y_i)(y_i - \mu)^2}{\sum_{i \in S} P^{(l)}(l|y_i)}} \tag{3.7}$$

[100] provides more detailed mathematical analysis of the HMRF-EM framework; Algorithm 2 depicts the pseudocode of the HMRF-EM framework.

This framework works well for small data dimensions and small amount of missing data. Its main advantages are: easy to implement, provides an accurate segmentation, and it is less sensitive to noise compared with other segmentation techniques, as clustering and classification, since it considers contextual information [97]. On the other hand, it has two main limitations. First, it is a time consuming algorithm, which prohibit its practical use [67]. Second, the selection of the parameters controls the strength of the spatial interaction. Therefore, an accurate selection is a must; otherwise an excessive smooth segmentation would be obtained which would discard some important structural details.

3.3 Proposed Segmentation Algorithm

The proposed CA segmentation algorithm starts by feeding a series of 2D images, of a certain patient, in the Digital Imaging and Communications in Medicine (DICOM) format. These images represent the Region of Interest (ROI), which consists of an aneurysm and some surrounding vessels; the selection of the ROI, from the entire cerebral vasculature, is done manually. Later, the following two main phases are performed consecutively on each 2D image separately.

During the **first phase**, CT is applied to extract features from an image by decomposing an image into 6 pyramidal levels and different number of directions for each level, where the number of the directional decomposition at each pyramidal level (from coarse to fine) are: 2^2, 2^2, 4^2, 4^2, 8^2, and 8^2 [40, 69, 85]; and as mentioned before in section 3.2.1, CT consists of two main filters to do its job and reach its goal, which are LP and DFB. A ladder filter, known as PKVA filter, is selected for the first filter. This filter, proposed by Phoonget al. [68], is more effective than other filters (e.g., CD) to localize edge direction as it reduces the inter-direction mutual information [69]. As for the second filter, $9-7$ bi-orthogonal Daubechies filter, known as $9-7$ (or 9/7) filter, is selected. This filter, introduced by Cohen and Daubechies [18], reduces significantly all the inter-scale, inter-location, and inter-direction mutual information of the contourlet; in addition, it is superior to other filters (e.g., the Haar filters) in terms of whitening the contourlet coefficients [69].

After the decomposition is done, using CT, only the lowpass subband image is selected, which consists of the coarsest produced coefficients since they are considered as the best representatives of all the produced coefficients to perform on them the remaining steps [69].

In order to apply the second phase of the segmentation algorithm, which is

the HMRF-EM, two prior steps need to be performed. The first step is to obtain a constrained image by applying a Canny edge detection operator to highlight the image's edges, since this operator produces thicker edges than the second derivative edge detection operator (e.g., LP) [9]. As for the second step, the initial segmentation and parameters, which are mainly the means and standard deviations, need to be initialized. Due to the over-estimation of the HMRF-EM framework [5], a technique with under-estimation is preferable to complement it. Accordingly, a k-means clustering is selected and applied [5]. The equation 3.8 illustrates the mathematical formula of this adopted clustering technique;

$$k - means = \sum_{i=1}^{k} \sum_{x_i \in S_i} (x_j - \mu_i)^2 \tag{3.8}$$

; and as we are targeting a full automatic approach, the selection of the number of clusters, k, is done automatically based on the image entropy. In this context, the entropy is a statistical measure of randomness that can be used to characterize the texture of a gray-scale image; in other words, it measures the amount of disorder in an image, which helps to determine the number of the needed clusters; equation 3.9 illustrates its formula.

$$entropy = -\sum_{i=0}^{n-1} P(x_i) \times \log_2 P(x_i) \tag{3.9}$$

The **second main phase** of the proposed algorithm, which is the HMRF-EM technique, starts now after getting all the needed inputs which are: the initial segmentation and the initial parameters obtained by the k-means clustering technique, the constrained image obtained by the Canny edge operator, and the lowpass subband image obtained by the contourlet decomposition. During this phase, the algorithm iterates between the E-Step and M-Step to enhance the initial segmented image, constrained by the canny segmented image, to

Algorithm 3 Proposed Algorithm for Cerebral Aneurysm Segmentation

```
Read DICOM images of a dataset and store them in V1
Select ROI from V1 and store them in V2
for each img ∈ V2 do
    Apply CT to decompose img and extract the coarsest coefficients
    Initialize the number of clusters k based on the image entropy
    Apply k-means on the coarsest coefficients
    Apply canny edge operator on the coarsest coefficients
    Apply HMRF-EM algorithm to get the final segmentation
    Reconstruct the image by applying the ICT
end for
Reconstruct the 3D segmented volume V3
```

end up with the final segmented 2D image by minimizing the posterior energy function as explained in section 3.2.2.

As the last step, Inverse Contourlet Transform (ICT) is applied to reconstruct the image and return it back to its original size. Here, the lowpass subband image, which represents the coarsest contourlet coefficients, is replaced by the final segmented image. The ICT is achieved using the same filters as in the decomposition stage, where the $9-7$ and PKVA filters are used for the LP and DFB respectively. Here, we apply the stages in the reverse order where the DFB phase is applied first followed later by the LP phase.

After completing these two main phases, a reconstruction, of all the segmented 2D images, is done to get the final segmented 3D volume of the ROI, which will be analyzed by the radiologist(s). The pseudocode for the overall proposed CA segmentation algorithm is presented in Algorithm 3; As in figure 3.6, the resulted images of each intermediate step are illustrated.

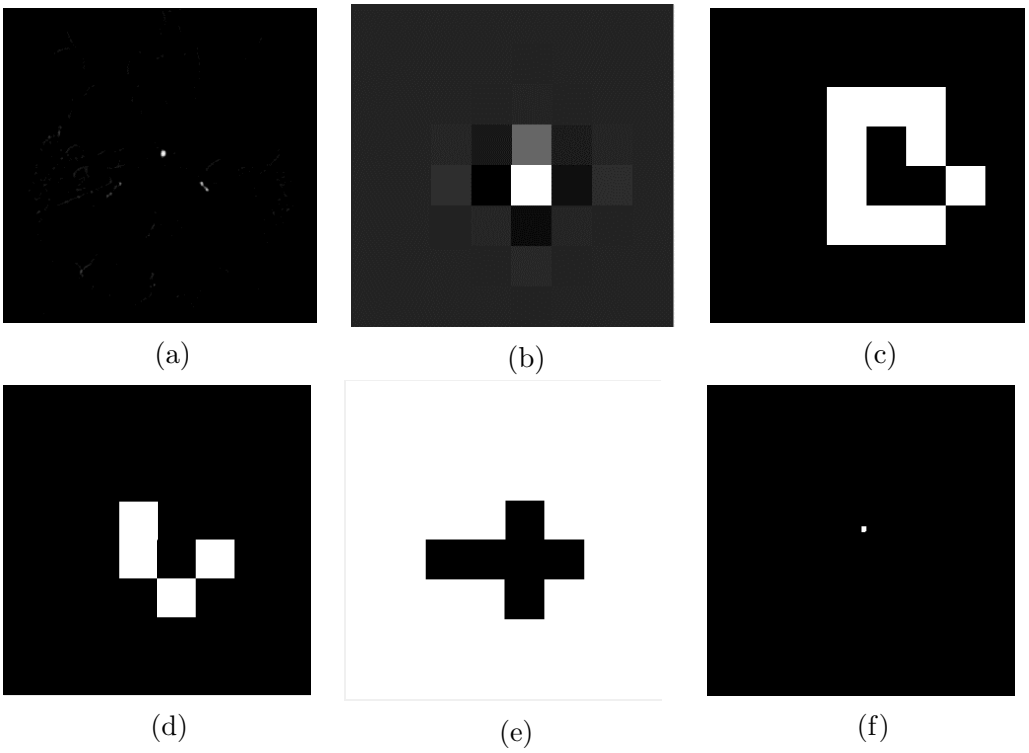

Figure 3.6: The resulted images of each intermediate step in the proposed algorithm: (a) 512x512 original 2D image (b) 8x8 lowpass subband 2D image after applying the CT decomposition (c) 8x8 constrained 2D image after applying the canny edge operator (d) 8x8 initial segmented 2D image after applying the k-means clustering technique (e) 8x8 HMRF-EM (f) 512x512 final segmented 2D image after applying ICT reconstruction

3.4 Summary

This chapter focuses on the proposed CA segmentation algorithm using the CT and HMRF-EM techniques, where a solid mathematical foundation is established for both of them. In the following chapter, this algorithm is evaluated objectively and subjectively on four datasets.

Chapter 4: Evaluation

This chapter establishes and reports everything related to the evaluation step to verify the robustness of the proposed algorithm to segment a Cerebral Aneurysm (CA), where different methods may be followed. In this thesis, an objective and subjective evaluation are carried out.

Section 4.1 introduces the used datasets in this thesis. Section 4.2 presents the environmental setup to implement and evaluates the proposed algorithm. Section 4.3 reports the final obtained results.

4.1 Datasets

The algorithm' s input is a dataset/series of images of a specific patient in the Digital Imaging and Communications in Medicine (DICOM), where DICOM is a standard format to store and manage medical images. This format groups much information about the image as the patient information and pixel data. The source of these images is one of the available acquisition scanners (or modalities). These scanners slice an object in a Two-Dimensional (2D) physical sectioning and stack them in parallel to form a Three-Dimensional (3D) volume. In our work, the datasets are acquired from a 3D Rotational Angiography (RA) modality.

3D RA technique depicts considerably small aneurysms ($\leq$ 3 millimeters) as it produces images with a very high contrast between blood vessels and the surrounding environment (bony or dense soft tissue environment). This contrast

is obtained by subtracting two images: The first image is acquired by injecting a contrast agent through a catheter into one of the vessels that leads to the brain vessels; while the second one is obtained before injecting this agent. Its accurate detection affects positively the choice of treatment technique; therefore, it is recommended to adopt 3D RA to detect and plan for the treatment accordingly [86].

Four 3D RA datasets are provided by Hamad Medical Corporation (HMC) to apply the proposed segmentation on them; each dataset consists of 385 2D slices of size 512×512 each. In addition, each dataset comes along with its ground truth data, which is a manual segmentation done by some experts in the field, to evaluate the segmentation performance. The provided ground truth data is in STL format, which is a widely used format for rapid prototyping, 3D printing, and computer-aided manufacturing [17]. STL describes only the surface geometry of a 3D object without any representation of texture, color, or other common CAD model attributes and it can be represented in both ASCII and binary encoding.

4.2 Environmental Setup

In order to implement the proposed algorithm, MATLAB R2017b is the software used running on a 64-bit Windows operating system machine with an i7 Intel core and a 16 GB RAM. Particularly, the following three toolboxes are used in the MATLAB environment:

1. Image Processing Toolbox: This toolbox extends MATLAB to help in working interactively with images by providing a set of functions and applications as segmentation, quality enhancement by noise removal, transformation to detect and measure features, and registration of multiple images into a common view to enable comparison or integration.

2. Contourlet Transform Toolbox: It is a free available toolbox in the MATLAB central developed by Do [21]. This toolbox provides a set of functions related to the contourlet process.

3. Hidden Markov Random Field with Expectation Maximization Toolbox: It is a free available toolbox in the MATLAB central developed by Wang [88], which provides the implementation of the HMRF-EM framework in the 2D domain.

4.3 Results

In order to obtain the results, a preliminary step is crucial to allow/permit the comparison between the segmented volume and the ground truth data. This step, which is the registration, is discussed in subsection 4.3.1. Later, the quantitative and qualitative results, obtained by comparing between the registered segmented volume and the ground truth volume, are elaborated in Section 4.3.2 and 4.3.3 respectively. Figure 4.1, 4.2, 4.3, and 4.4 depict each dataset before and after applying the segmentation.

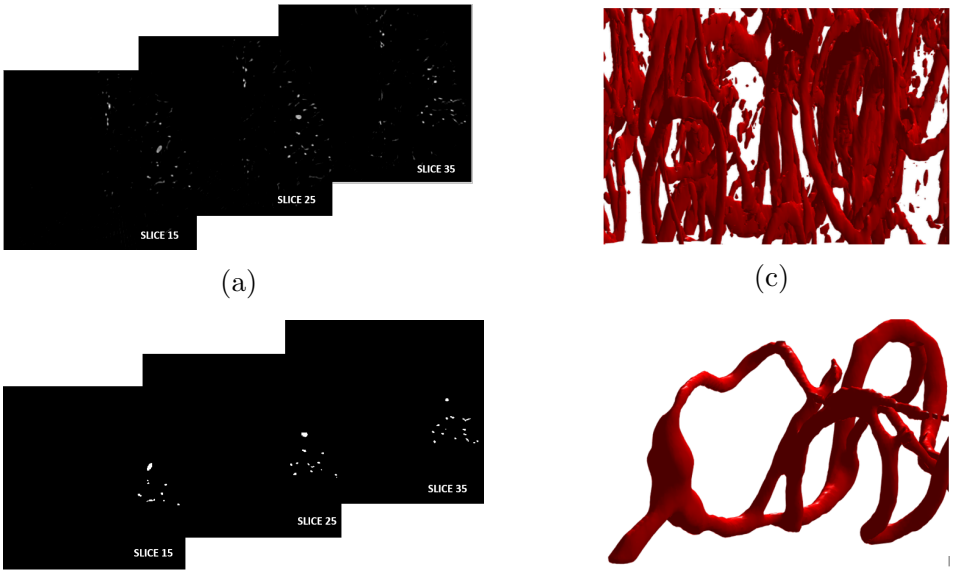

(a) (c)

(b) (d)

Figure 4.1: From ROI of dataset 1: Left column depicts three slices (a) before segmentation (b) after segmentation. Right column depicts the ROI's volume (c) before segmentation (d) after segmentation

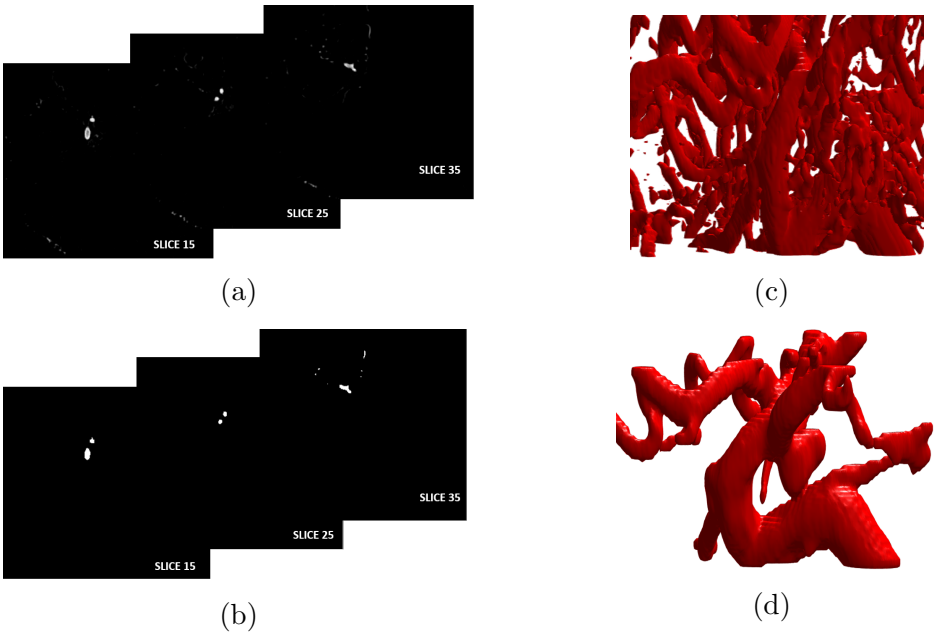

(a) (c)

(b) (d)

Figure 4.2: From ROI of dataset 2: Left column depicts three slices (a) before segmentation (b) after segmentation. Right column depicts the ROI's volume (c) before segmentation (d) after segmentation

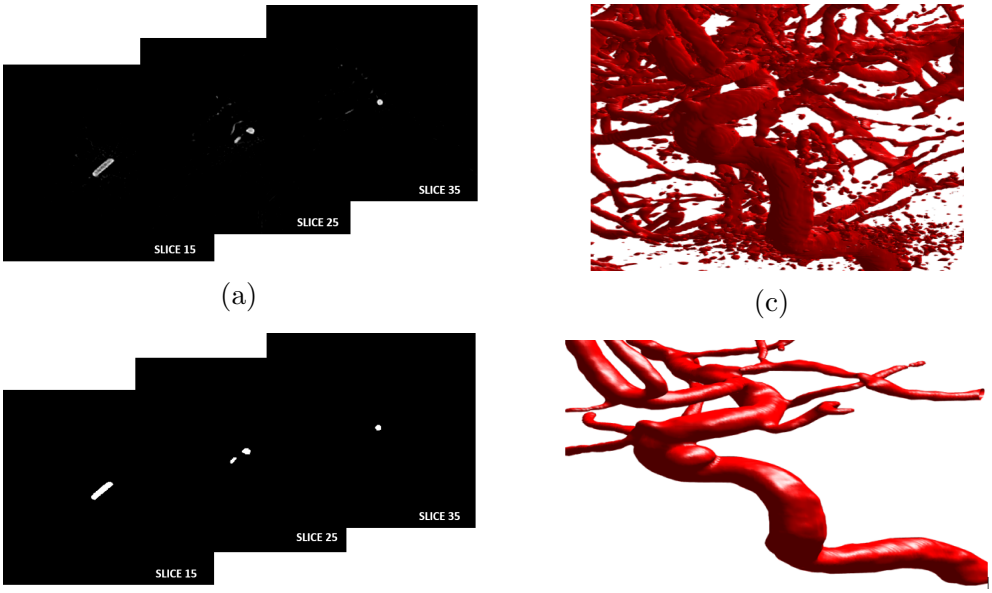

(a) (c)

(b) (d)

Figure 4.3: From ROI of dataset 3: Left column depicts three slices (a) before segmentation (b) after segmentation. Right column depicts the ROI's volume (c) before segmentation (d) after segmentation

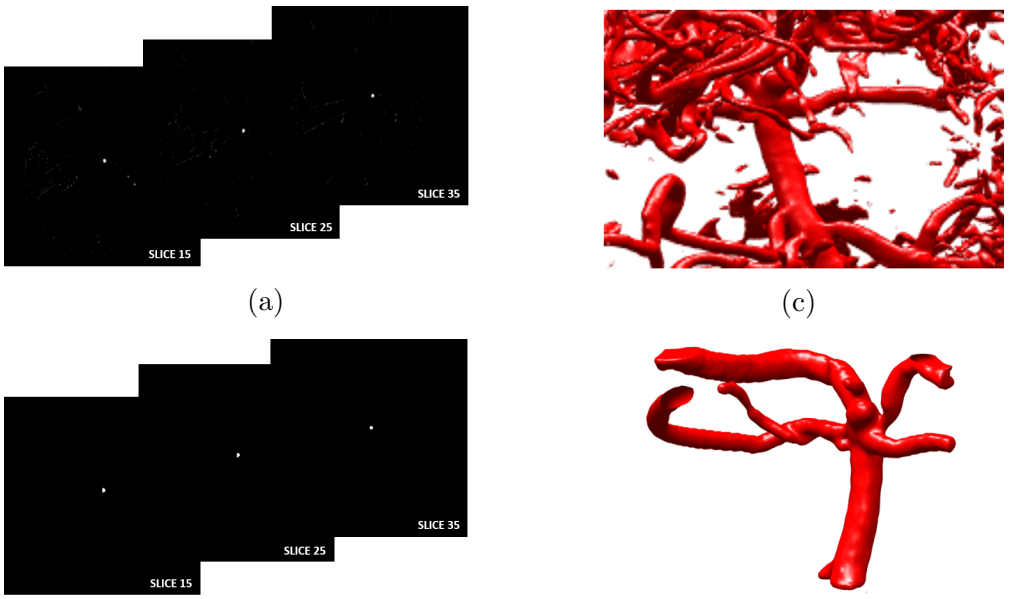

(a) (c)

(b) (d)

Figure 4.4: From ROI of dataset 4: Left column depicts three slices (a) before segmentation (b) after segmentation. Right column depicts the ROI's volume (c) before segmentation (d) after segmentation

4.3.1 Registration

Registration is process of aligning two (or more) images of the same scene, in 2D or 3D spatial domain, taken in different conditions: different sensors, at different times, different depths, or different viewpoints, etc. These differences prevent the possibility of comparing these images [101]. Therefore, image registration is an important step to allow the comparison or the integration of different datasets. Figure 4.5 depicts the difference between the coordinate system of the original dataset and the ground truth data. Therefore, the registration is crucial in this work to enable the comparison between the segmented volume, in the DICOM format, and the ground truth volume, in the STL format.

In this process, one of the images is defined as the target (or the subject), which we wish to apply a transformation on it. While the other image is defined as the reference (or the source) against, which we aim to register the other image it. In our case, the target image is the segmented ROI volume; while the reference image is the ground truth ROI volume. The target image is transformed by means of the selected mapping functions to align it with the reference image [101]. Different mapping functions exist (e.g., affine, rigid, translation, similarity transformations [1]), where each one offers different geometric deformations/transformations or local displacements. Therefore, the selection should be selected according to the desired deformation. In this work, an affine transformation is selected as it satisfies the need for the translation and scaling. Figure 4.6 illustrates, for one dataset as an example, the similarity between the coordinate systems of the segmented volume and the ground truth data after registration and the ground truth data.

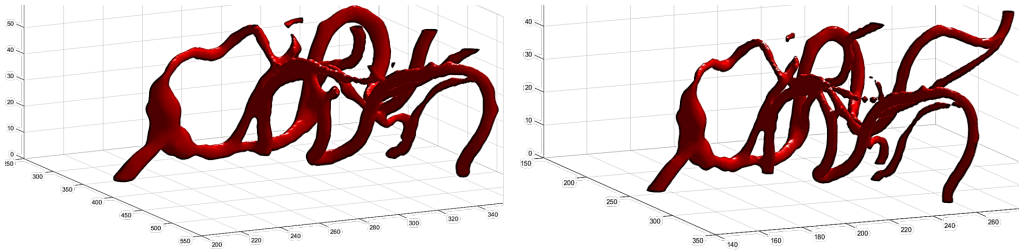

(a) The whole volume

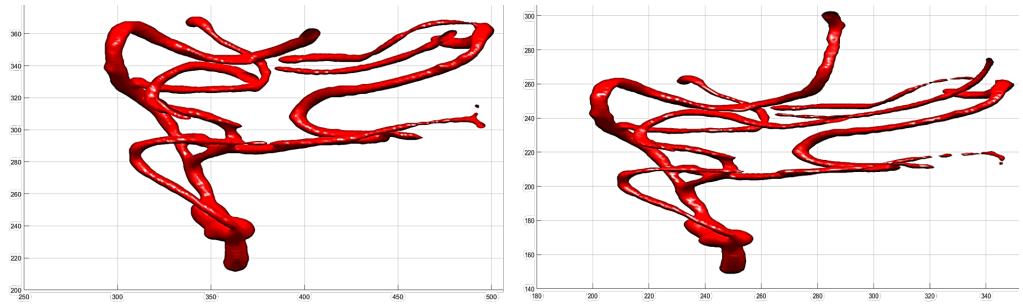

(b) X —Y axis

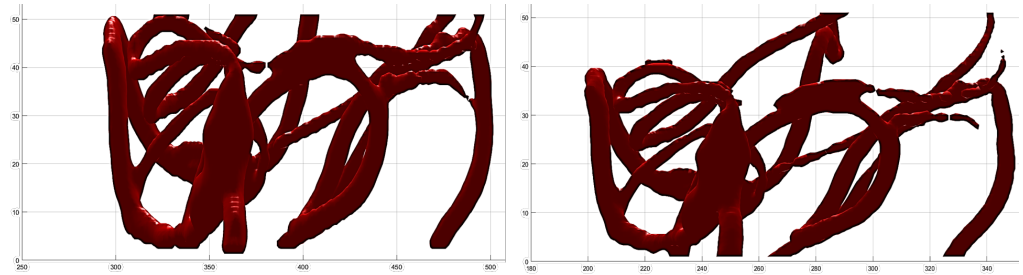

(c) X —Z axis

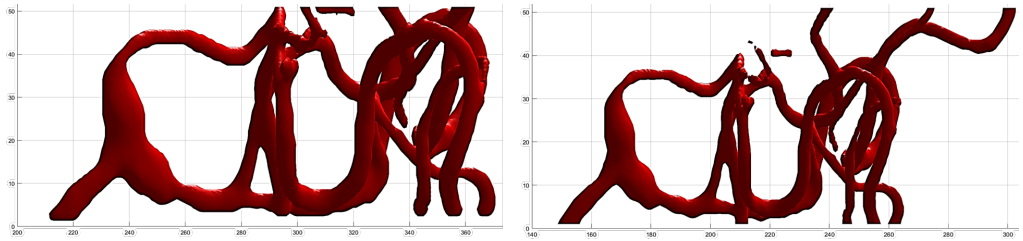

(d) Y —Z axis

Figure 4.5: Coordinate system of dataset 1 before registration. The right column is related to the ground truth data. The left column is related to the original segmented ROI volume

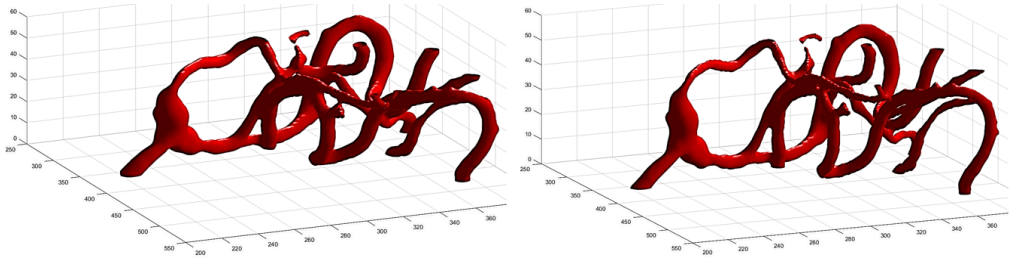

(a) The whole volume

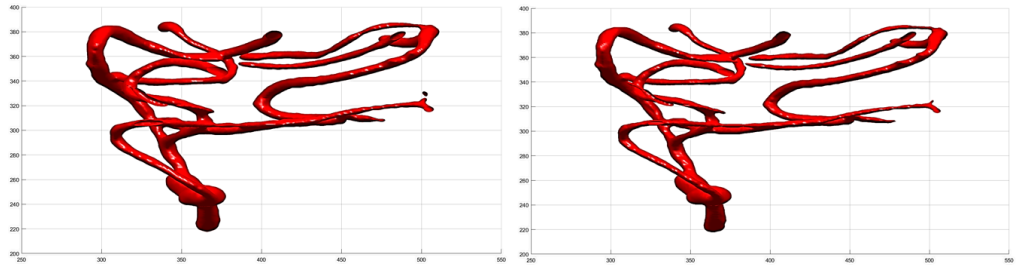

(b) X —Y axis

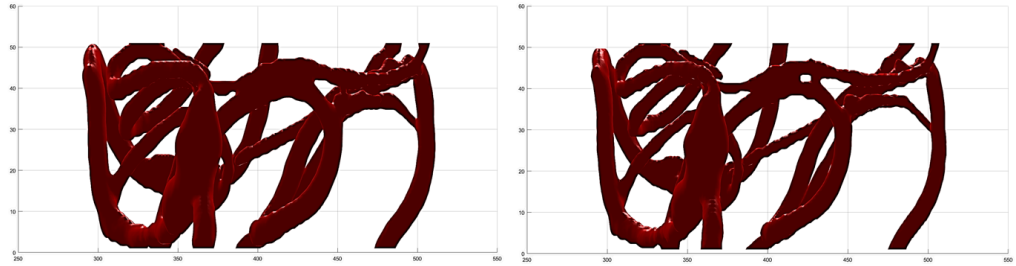

(c) X —Z axis

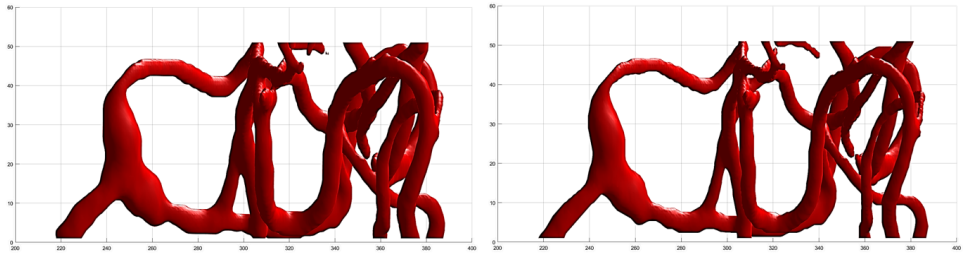

(d) Y —Z axis

Figure 4.6: Coordinate system of dataset 1 after registration. The right column is related to the ground truth data. The left column is related to the registered segmented volume

4.3.2 Objective Evaluation

Six performance metrics are used to measure the proposed CA segmentation quantitatively which are: accuracy, Dice Similarity Index (DSI), False Positive Ratio (FPR), False Negative Ratio (FNR), sensitivity, and specificity. The value of these metrics ranges between 0 and 1. Table 4.1 depicts the definition and the formula of each metric.

In all the illustrated equations in Table 4.1, four measures are used: True Positive (TP) and True Negative (TN) which indicate a correct segmentation. While False Positive (FP) and False Negative (FN) indicate an incorrect segmentation. Figure 4.7 depicts the meaning of each measure more clearly.

These introduced performance metrics are calculated and reported in Table 4.2 for each dataset.

4.3.3 Subjective Evaluation

Each dataset is accessed visually by five observers, where one of them is an expert in the domain and the rest have some medical background. A rate, ranging between 0 and 5, is assigned by each observer, where 5 means that the ground truth volume and the segmented volume are identical. While 0 means completely the opposite. Table 4.3 reports the observations for the four datasets.

4.4 Summary

This chapter reports the objective and subjective evaluation results of the proposed CA segmentation algorithm. In the following Chapter 5, a discussion of these results is elaborated, where some future works are pointed out.

Table 4.1: Six adopted performance metrics for the quantitative evaluation

Performance Metric	Definition	Equation
Accuracy	Correctness of the overall segmentation	$\frac{TP+TN}{TP+TN+FP+FN}$
DSI	Amount of overlap between the two segmentation	$\frac{2\times TP}{2\times TP+FP+FN}$
False Positive Rate	Number of pixels incorrectly segmented	$\frac{FP}{FP+TN} = 1 - Specificity$
False Negative Rate	Number of pixels incorrectly rejected	$\frac{FN}{FN+TP} = 1 - Sensitivity$
Sensitivity	Number of pixels segmented correctly	$\frac{TP}{TP+FN}$
Specificity	Number of pixels excluded correctly	$\frac{TN}{TN+FP}$

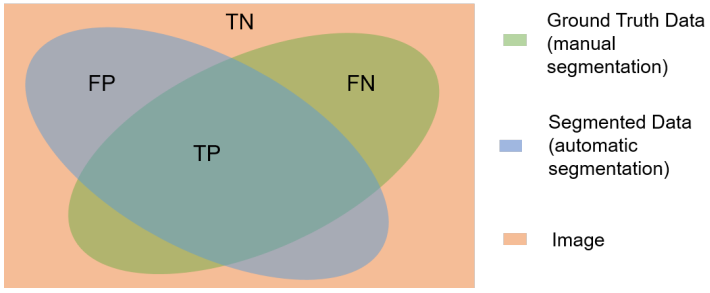

Figure 4.7: Four measures used in the six adopted performance metrics

Table 4.2: Objective evaluation results

	Dataset 1	Dataset 2	Dataset 3	Dataset 4	Average
Accuracy (%)	99.99	99.92	99.78	99.75	**99.86**
Sensitivity (%)	98.84	96.42	97.20	86.44	**94.73**
Specificity (%)	99.99	99.94	99.83	99.92	**99.92**
DSI (%)	97.46	93.15	94.13	89.56	**93.58**
FPR (%)	0.01	0.06	0.17	0.08	**0.08**
FNR (%)	1.16	3.58	2.8	13.56	**5.27**

Table 4.3: Subjective evaluation results

	Dataset 1	Dataset 2	Dataset 3	Dataset 4	Average
Observer 1	5	4	4	3	4
Observer 2	5	4	5	3	4.25
Observer 3	5	4	5	4	4.5
Observer 4	5	4	4	4	4.25
Observer 5	5	4	5	3	4.25
					4.25

Chapter 5: Conclusion

5.1 'Revisited' Research Objectives and Contribution

The objectives of this thesis presented in section 1.3, are revisited again to determine if it is addressed successfully.

1. **Has an intensive literature review of different Medical Image Segmentation (MIS) techniques and different existing Cerebral Aneurysm (CA) segmentation algorithms been carried out?**
   Chapter 2 has successfully satisfied this objective. Section 2.1 has presented and reviewed different MIS techniques, which have been categorized into seven groups. As in Section 2.2, different recently developed CA segmentation algorithms have been presented and discussed in terms of their methodology, the needed user intervention, their limitations, the adopted modalities etc.

2. **Has an automatic CA segmentation algorithm been developed?**
   A new promising and robust automatic CA segmentation algorithm has been developed using multiresolution and statistical approaches in Two-Dimensional (2D) domain. CT, which has been selected as a multiresolution analysis technique, extracts image' s features not apparent in the normal scale. As the HMRF-EM framework, which has been selected as a statistical approach, models the relationship of neighboring pixels in the contourlet domain to capture the spatial contextual constraints,

where correlated neighboring pixels are categorized into the same partition/region. Chapter 3 discusses in details the methodology of this proposed algorithm.

3. **Has the developed CA segmentation algorithm been evaluated objectively and subjectively?**

   Chapter 4 has successfully satisfied this objective. Section 4.3.2 has reported the quantitative results of six adopted performance metrics. As Section 4.3.3 has reported the qualitative results of five visual observations, where the observers have been selected as follow: one expert in the domain (a neuroradiologist) and four observers with some medical background.

5.2 Research Discussion and Future Work

Sub-Arachnoid Hemorrhage (SAH), caused by a ruptured CA, is a serious condition associated with high rates of morbidity and mortality. Therefore, detecting and diagnosing CAs at an early stage is imperative. In this work, an automatic CA segmentation algorithm is developed using CT, as a multiresolution technique, and HMRF-EM, as a statistical approach. In addition, Canny edge-based and k-means clustering-based segmentation techniques are used along with the main adopted ones.

This developed algorithm reveals promising quantitative and qualitative results on the four tested Three-Dimensional Rotational Angiography (3D RA) datasets. For the quantitative evaluation, an average of 99.86% accuracy, 93.58% Dice Similarity Index, 0.08% False Positive Ratio, 5.27% False Negative Ratio, 99.92% specificity, and 94.73% sensitivity were achieved. As for the qualitative evaluation, an average of 4.25 over 5 is obtained. However, as illustrated in the Tables 4.2 and 4.3, the last dataset has the worst results

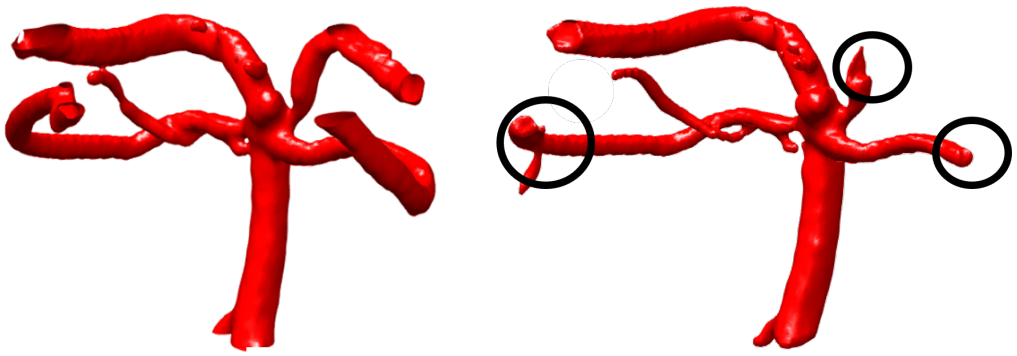

(a) (b)

Figure 5.1: Dataset 4 (a) Segmented volume from the original DICOM dataset (b) Ground truth volume delineated by the experts

compared to the remaining datasets in both the quantitative and qualitative evaluation. These results are obtained due to the fact that the provided ground truth data does not involve the complete brain vessels tree and only a delineated ROI is provided, where some surrounding vessels are cutout. This fact affects the evaluation, as some visible vessels in the segmented ROI are cropped by the experts in the ground truth ROI. Figure 5.1 illustrates more clearly the above-explained condition of the last dataset.

Therefore, more datasets need to be involved in the evaluation phase in order to confirm the robustness and the reliability of the proposed CA segmentation algorithm in the clinical practice. In addition, the qualitative evaluation would most probably be better if more experts are engaged in this process to avoid the bias results.

The computational time needed to segment is considerably fast, knowing that HMRF suffers from its intensive computation [67]; but adopting the multiresolution analysis technique, CT, helps in overcoming this downside as it decomposes the image into different resolutions and HMRF is only applied on a

Table 5.1: Time consumption to segment CA using the proposed approach

	Dataset 1	Dataset 2	Dataset 3	Dataset 4	Average
Segmenting ROI in sec	32.12	28.56	93.46	57.56	**52.93**
	(51 slices)	(51 slices)	(161 slices)	(80 slices)	**(86 slices)**
Segmenting the whole volume in min	4.38	3.21	3.3	5.31	**4.05**
	(385 slices)	(385 slices)	(385 slices)	(385 slices)	**(385 slices)**

reduced scale. Table 5.1 reports the running time of the proposed segmentation algorithm for the whole volume, in minutes, as well as for the ROI, in seconds. However, an acceleration can be adopted to increase the efficiency of the developed algorithm, to guarantee its applicability in real-time clinical practices, using Field-Programmable Gate Array (FPGAs) or Graphics Processing Unit (GPUs) which are adopted already in different works and proved their feasibility [28, 36, 78, 84].

Moreover, since the algorithm is tested only on 3D RA datasets, different modalities can be used to check their compatibility (e.g., CTA and MRA) since they are commonly used to detect and diagnosis CAs. Furthermore, the algorithm can be tested on datasets with a treated CA (e.g. after placing the blood flow diverters, clip, or coil) to examine the treated aneurysm and assess the success of the surgery to act accordingly.

Bibliography

[1] Registering multimodal mri images. `http://www.mathworks.com/help/images/registering-multimodal-mri-images.html`. Accessed: 2017-08-15.

[2] Hayder Saad Abdulbaqi, Mohd Zubir Mat Jafri, Ahmad Fairuz Omar, Kussay N Mutter, Loay Kadom Abood, and Iskandar Shahrim Bin Mustafa. Segmentation and estimation of brain tumor volume in computed tomography scan images using hidden markov random field expectation maximization algorithm. In *Research and Development (SCOReD), 2015 IEEE Student Conference on*, pages 55–60. IEEE, 2015.

[3] Ahmad Alzubi, Abbes Amira, and Naeem Ramzan. Semantic content-based image retrieval: A comprehensive study. *Journal of Visual Communication and Image Representation*, 32:20–54, 2015.

[4] Shadi AlZu'bi and Abbes Amira. 3d medical volume segmentation using hybrid multiresolution statistical approaches. *Advances in Artificial Intelligence*, 2010, 2010.

[5] Shadi AlZubi, Naveed Islam, and Maysam Abbod. Multiresolution analysis using wavelet, ridgelet, and curvelet transforms for medical image segmentation. *Journal of Biomedical Imaging*, 2011:4, 2011.

[6] Abbes Amira, Shrutisagar Chandrasekaran, David WG Montgomery, and Isa Servan Uzun. A segmentation concept for positron emission

tomography imaging using multiresolution analysis. *Neurocomputing*, 71(10):1954–1965, 2008.

[7] Praylin Selva Blessy Selvaraj Assley and Helen Sulochana Chellakkon. A comparative study on medical image segmentation methods. *Applied Medical Informatics*, 34(1):31, 2014.

[8] Roberto H Bamberger and Mark JT Smith. A filter bank for the directional decomposition of images: Theory and design. *IEEE transactions on signal processing*, 40(4):882–893, 1992.

[9] Saket Bhardwaj and Ajay Mittal. A survey on various edge detector techniques. *Procedia Technology*, 4:220–226, 2012.

[10] Yuri Boykov, Olga Veksler, and Ramin Zabih. Fast approximate energy minimization via graph cuts. *IEEE Transactions on pattern analysis and machine intelligence*, 23(11):1222–1239, 2001.

[11] Jonathan L Brisman, Joon K Song, and David W Newell. Cerebral aneurysms. *New England Journal of Medicine*, 355(9):928–939, 2006.

[12] Peter Burt and Edward Adelson. The laplacian pyramid as a compact image code. *IEEE Transactions on communications*, 31(4):532–540, 1983.

[13] Bin Chen, Yang Chen, Guanyu Yang, Jingyu Meng, Rui Zeng, and Limin Luo. Segmentation of liver tumor via nonlocal active contours. In *Image Processing (ICIP), 2015 IEEE International Conference on*, pages 3745–3748. IEEE, 2015.

[14] SY Chen, Hanyang Tong, and Carlo Cattani. Markov models for image labeling. *Mathematical Problems in Engineering*, 2012, 2011.

[15] Yu Chen, Laurent Navarro, Yan Wang, and Guy Courbebaisse. Segmentation of the thrombus of giant intracranial aneurysms from ct angiography scans with lattice boltzmann method. *Medical image analysis*, 18(1):1–8, 2014.

[16] MC Jobin Christ and RMS Parvathi. Fuzzy c-means algorithm for medical image segmentation. In *Electronics Computer Technology (ICECT), 2011 3rd International Conference on*, volume 4, pages 33–36. IEEE, 2011.

[17] Chee Kai Chua, Kah Fai Leong, and Chu Sing Lim. pages 301–302. Am Soc Neuroradiology, 2010.

[18] Albert Cohen and Ingrid Daubechies. Non-separable bidimensional. *Revista Matematica Iberoamericana*, 9(1), 1993.

[19] Sarada Prasad Dakua, Julien Abinahed, and Abdulla Al-Ansari. A pca-based approach for brain aneurysm segmentation. *Multidimensional Systems and Signal Processing*, pages 1–21, 2016.

[20] Sudeb Das and Malay Kumar Kundu. Fusion of multimodality medical images using combined activity level measurement and contourlet transform. In *Image Information Processing (ICIIP), 2011 International Conference on*, pages 1–6. IEEE, 2011.

[21] Minh Do. Contourlet toolbox - file exchange - matlab central. `https://www.mathworks.com/matlabcentral/fileexchange/8837-contourlet-toolbox`. Accessed: 2017-02-20.

[22] Minh N Do. Directional multiresolution image representations. 2002.

[23] Minh N Do and Martin Vetterli. Pyramidal directional filter banks and curvelets. In *Image Processing, 2001. Proceedings. 2001 International Conference on*, volume 3, pages 158–161. IEEE, 2001.

[24] Minh N Do and Martin Vetterli. Contourlets: a directional multiresolution image representation. In *Image Processing. 2002. Proceedings. 2002 International Conference on*, volume 1, pages I–I. IEEE, 2002.

[25] Minh N Do and Martin Vetterli. 4-contourlets. *Studies in computational mathematics*, 10:83–105, 2003.

[26] Minh N Do and Martin Vetterli. The contourlet transform: an efficient directional multiresolution image representation. *IEEE Transactions on image processing*, 14(12):2091–2106, 2005.

[27] Duc M Duong and Duc A Duong. Robust and high capacity watermaking scheme for medical images based on contourlet transform. In *Systems and Informatics (ICSAI), 2012 International Conference on*, pages 2183–2187. IEEE, 2012.

[28] Anders Eklund, Paul Dufort, Daniel Forsberg, and Stephen M LaConte. Medical image processing on the gpu–past, present and future. *Medical image analysis*, 17(8):1073–1094, 2013.

[29] Salvador Espana-Boquera, Maria Jose Castro-Bleda, Jorge Gorbe-Moya, and Francisco Zamora-Martinez. Improving offline handwritten text recognition with hybrid hmm/ann models. *IEEE transactions on pattern analysis and machine intelligence*, 33(4):767–779, 2011.

[30] Pedro F Felzenszwalb and Daniel P Huttenlocher. Image segmentation using local variation. In *Computer Vision and Pattern Recognition, 1998.*

Proceedings. 1998 IEEE Computer Society Conference on, pages 98–104. IEEE, 1998.

[31] Azadeh Firouzian, Rashindra Manniesing, Zwenneke H Flach, Roelof Risselada, Fop van Kooten, Miriam CJM Sturkenboom, Aad van der Lugt, and Wiro J Niessen. Intracranial aneurysm segmentation in 3d ct angiography: Method and quantitative validation with and without prior noise filtering. *European journal of radiology*, 79(2):299–304, 2011.

[32] Riad Gobran, Ajay Wakhloo, and Yusuf Khan. Blood flow diverters for the treatment of intracranial aneurysms, June 22 2004. US Patent App. 10/874,639.

[33] Rafael C Gonzalez and Richard E Woods. *Digital image processing*. Pearson, 2017.

[34] Nelly Gordillo, Eduard Montseny, and Pilar Sobrevilla. State of the art survey on mri brain tumor segmentation. *Magnetic resonance imaging*, 31(8):1426–1438, 2013.

[35] Leo Grady. Random walks for image segmentation. *IEEE transactions on pattern analysis and machine intelligence*, 28(11):1768–1783, 2006.

[36] Markus Hadwiger, Caroline Langer, Henning Scharsach, and Katja Buhler. State of the art report 2004 on gpu-based segmentation. *VRVis Research Center*, 3, 2004.

[37] SeyyedHadi Hashemi-Berenjabad, Ali Mahloojifar, and Amir Akhavan. Threshold based lossy compression of medical ultrasound images using contourlet transform. In *Biomedical Engineering (ICBME), 2011 18th Iranian Conference of*, pages 191–194. IEEE, 2011.

[38] Clemens M Hentschke, Oliver Beuing, Harald Paukisch, Cordula Scherlach, Martin Skalej, and Klaus D Tönnies. A system to detect cerebral aneurysms in multimodality angiographic data sets. *Medical physics*, 41(9), 2014.

[39] Randall T Higashida. What you should know about cerebral aneurysms. *Pamphlet. American Heart Association Cardiovascular Council*, 2003.

[40] PS Hiremath, Prema T Akkasaligar, and Sharan Badiger. Speckle reducing contourlet transform for medical ultrasound images. *Int J Compt Inf Engg*, 4(4):284–291, 2010.

[41] D Jayadevappa, S Srinivas Kumar, and DS Murty. Medical image segmentation algorithms using deformable models: a review. *IETE Technical review*, 28(3):248–255, 2011.

[42] Aiping Jiang, Ping Ren, and Pingyuan Yang. Medical image enhancement algorithm based on contourlet transform. In *Pervasive Computing Signal Processing and Applications (PCSPA), 2010 First International Conference on*, pages 624–627. IEEE, 2010.

[43] Juilee Katkar, Trupti Baraskar, and Vijay R Mankar. A novel approach for medical image segmentation using pca and k-means clustering. In *Applied and Theoretical Computing and Communication Technology (iCATccT), 2015 International Conference on*, pages 430–435. IEEE, 2015.

[44] Abhinav Krishn, Vikrant Bhateja, Akanksha Sahu, et al. Pca based medical image fusion in ridgelet domain. In *Proceedings of the 3rd International Conference on Frontiers of Intelligent Computing: Theory and Applications (FICTA) 2014*, pages 475–482. Springer, 2015.

[45] Kelly Lake. Pegasus therapeutics - healing kids with aneurysms. https://www.indiegogo.com/projects/pegasus-therapeutics-healing-kids-with-aneurysms#/, 2015. Accessed: 2017-09-31.

[46] Alexandra Lauric, Eric Miller, Sarah Frisken, and Adel M Malek. Automated detection of intracranial aneurysms based on parent vessel 3d analysis. *Medical image analysis*, 14(2):149–159, 2010.

[47] Alexandra Lauric, Eric L Miller, Merih I Baharoglu, and Adel M Malek. 3d shape analysis of intracranial aneurysms using the writhe number as a discriminant for rupture. *Annals of biomedical engineering*, 39(5):1457–1469, 2011.

[48] Max WK Law and Albert CS Chung. Segmentation of intracranial vessels and aneurysms in phase contrast magnetic resonance angiography using multirange filters and local variances. *IEEE Transactions on image processing*, 22(3):845–859, 2013.

[49] David Lesage, Elsa D Angelini, Isabelle Bloch, and Gareth Funka-Lea. A review of 3d vessel lumen segmentation techniques: Models, features and extraction schemes. *Medical image analysis*, 13(6):819–845, 2009.

[50] Michael E Leventon, W Eric L Grimson, and Olivier Faugeras. Statistical shape influence in geodesic active contours. In *Computer Vision and Pattern Recognition, 2000. Proceedings. IEEE Conference on*, volume 1, pages 316–323. IEEE, 2000.

[51] Bing Nan Li, Chee Kong Chui, Stephen Chang, and Sim Heng Ong. Integrating spatial fuzzy clustering with level set methods for automated medical image segmentation. *Computers in biology and medicine*, 41(1):1–10, 2011.

[52] Qiao Li and Haiyun Li. A novel algorithm based on contourlet transform for medical image segmentation. In *Bioinformatics and Biomedical Engineering (iCBBE), 2010 4th International Conference on*, pages 1–3. IEEE, 2010.

[53] Hongying Liu, Yi Liu, Qian Li, Hongyan Liu, and Yongan Tong. Medical image segmentation based on contourlet transform and watershed algorithm. In *IT in Medicine and Education (ITME), 2011 International Symposium on*, volume 2, pages 224–227. IEEE, 2011.

[54] Vijay M Mane, DV Jadhav, and Akshay Bansod. An automatic approach to hemorrhages detection. In *Information Processing (ICIP), 2015 International Conference on*, pages 135–138. IEEE, 2015.

[55] Fatemeh Moayedi, Zohreh Azimifar, Reza Boostani, and Serajodin Katebi. Contourlet-based mammography mass classification using the svm family. *Computers in biology and medicine*, 40(4):373–383, 2010.

[56] Aisha Moin, Vikrant Bhateja, and Anuja Srivastava. Weighted-pca based multimodal medical image fusion in contourlet domain. In *Proceedings of the International Congress on Information and Communication Technology*, pages 597–605. Springer, 2016.

[57] Emanuele Monti, Valentina Pedoia, Elisabetta Binaghi, and Sergio Balbi. Study of the prognostic relevance of longitudinal brain atrophy in post-traumatic diffuse axonal injury using graph-based mri segmentation techniques. In *Computational Modeling of Objects Presented in Images*, pages 245–268. Springer, 2014.

[58] Alireza Nikravanshalmani, Mojdeh Karamimohammdi, and Jamshid Dehmeshki. Segmentation and separation of cerebral aneurysms: A

multi-phase approach. In *Image and Signal Processing and Analysis (ISPA), 2013 8th International Symposium on*, pages 505–510. IEEE, 2013.

[59] Alireza Nikravanshalmani, Salah D Qanadli, Tim J Ellis, Matthew Crocker, Yousef Ebrahimdoost, Mojdeh Karamimohammadi, and Jamshid Dehmeshki. Three-dimensional semi-automatic segmentation of intracranial aneurysms in cta. In *Information Technology and Applications in Biomedicine (ITAB), 2010 10th IEEE International Conference on*, pages 1–4. IEEE, 2010.

[60] Alireza Norouzi, Mohd Shafry Mohd Rahim, Ayman Altameem, Tanzila Saba, Abdolvahab Ehsani Rad, Amjad Rehman, and Mueen Uddin. Medical image segmentation methods, algorithms, and applications. *IETE Technical Review*, 31(3):199–213, 2014.

[61] Fatma Ouertani, Carlos Vazquez, Thierry Cresson, and Jacques de Guise. Simultaneous extraction of two adjacent bony structures in x-ray images: application to hip joint segmentation. In *Image Processing (ICIP), 2015 IEEE International Conference on*, pages 4555–4559. IEEE, 2015.

[62] Dinesh D Patil and Sonal G Deore. Medical image segmentation: a review. *International Journal of Computer Science and Mobile Computing*, 2(1):22–27, 2013.

[63] Dipti Patra and Smita Pradhan. Development of fuzzy clustering based unsupervised scheme for medical image segmentation using hmrf model. In *Industrial Electronics, Control & Robotics (IECR), 2010 International Conference on*, pages 225–229. IEEE, 2010.

[64] Massimiliano Pavan and Marcello Pelillo. A new graph-theoretic approach to clustering and segmentation. In *Computer Vision and Pattern*

Recognition, 2003. Proceedings. 2003 IEEE Computer Society Conference on, volume 1, pages I–I. IEEE, 2003.

[65] Massimiliano Pavan and Marcello Pelillo. Dominant sets and pairwise clustering. *IEEE transactions on pattern analysis and machine intelligence*, 29(1):167–172, 2007.

[66] Bo Peng, Lei Zhang, and David Zhang. A survey of graph theoretical approaches to image segmentation. *Pattern Recognition*, 46(3):1020–1038, 2013.

[67] Dzung L Pham, Chenyang Xu, and Jerry L Prince. Current methods in medical image segmentation 1. *Annual review of biomedical engineering*, 2(1):315–337, 2000.

[68] See-May Phoong, Chai W Kim, PP Vaidyanathan, and Rashid Ansari. A new class of two-channel biorthogonal filter banks and wavelet bases. *IEEE Transactions on Signal Processing*, 43(3):649–665, 1995.

[69] DD-Y Po and Minh N Do. Directional multiscale modeling of images using the contourlet transform. *IEEE Transactions on image processing*, 15(6):1610–1620, 2006.

[70] RJ Ramteke and Y Khachane Monali. Automatic medical image classification and abnormality detection using k-nearest neighbour. *International Journal of Advanced Computer Research*, 2(4):190–196, 2012.

[71] Maryam Rastgarpour and J Shanbehzadeh. Application of ai techniques in medical image segmentation and novel categorization of available methods and. In *Tools, Proceedings of the International MultiConference of Engineers and Computer Scientists 2011 Vol I, IMECS 2011, March 16-18, 2011, Hong Kong*. Citeseer, 2011.

[72] Johnson Renoh, Paul Veena, N Naveen, and J Padmagireesan. Curvelet transform based retinal image analysis. *International Journal of Electrical and Computer Engineering*, 3(3):366–371, 2013.

[73] Tarak Ben Said and Olfa Azaiz. Segmentation of liver tumor using hmrf-em algorithm with bootstrap resampling. In *I/V Communications and Mobile Network (ISVC), 2010 5th International Symposium on*, pages 1–4. IEEE, 2010.

[74] S Satheesh and KVSVR Prasad. Medical image denoising using adaptive threshold based on contourlet transform. *arXiv preprint arXiv:1103.4907*, 2011.

[75] SS Savkare and SP Narote. Blood cell segmentation from microscopic blood images. In *Information Processing (ICIP), 2015 International Conference on*, pages 502–505. IEEE, 2015.

[76] Yuka Sen, Yi Qian, Alberto Avolio, and Michael Morgan. Development of image segmentation methods for intracranial aneurysms. *Computational and mathematical methods in medicine*, 2013, 2013.

[77] E Sgouritsa, A Mohamed, H Morsi, H Shaltoni, Michel E Mawad, and Ioannis A Kakadiaris. Neck localization and geometry quantification of intracranial aneurysms. In *Biomedical Imaging: From Nano to Macro, 2010 IEEE International Symposium on*, pages 1057–1060. IEEE, 2010.

[78] Mhd S Sharif, Abdul N Sazish, and Abbes Amira. An efficient algorithm and architecture for medical image segmentation and tumour detection. In *Biomedical Circuits and Systems Conference, 2008. BioCAS 2008. IEEE*, pages 157–160. IEEE, 2008.

[79] Mhd Saeed Sharif, Maysam Abbod, Abbes Amira, and Habib Zaidi. Artificial neural network-based system for pet volume segmentation. *Journal of Biomedical Imaging*, 2010:4, 2010.

[80] Neeraj Sharma, Lalit M Aggarwal, et al. Automated medical image segmentation techniques. *Journal of medical physics*, 35(1):3, 2010.

[81] Jianbo Shi and Jitendra Malik. Normalized cuts and image segmentation. *IEEE Transactions on pattern analysis and machine intelligence*, 22(8):888–905, 2000.

[82] Navid Shiee, Pierre-Louis Bazin, Arzu Ozturk, Daniel S Reich, Peter A Calabresi, and Dzung L Pham. A topology-preserving approach to the segmentation of brain images with multiple sclerosis lesions. *NeuroImage*, 49(2):1524–1535, 2010.

[83] Bhupinder Singh, Neha Kapur, and Puneet Kaur. Speech recognition with hidden markov model: a review. *International Journal of Advanced Research in Computer Science and Software Engineering*, 2(3), 2012.

[84] Erik Smistad, Thomas L Falch, Mohammadmehdi Bozorgi, Anne C Elster, and Frank Lindseth. Medical image segmentation on gpus–a comprehensive review. *Medical image analysis*, 20(1):1–18, 2015.

[85] Vassilis Spiliotopoulos, Nikolaos D Zervas, Yiannis Andreopoulos, G Anagnostopoulos, and Costas E Goutis. Quantization effect on vlsi implementations for the 9/7 dwt filters. In *Acoustics, Speech, and Signal Processing, 2001. Proceedings.(ICASSP'01). 2001 IEEE International Conference on*, volume 2, pages 1197–1200. IEEE, 2001.

[86] Willem Jan van Rooij, ME Sprengers, Anjob N de Gast, JPP Peluso, and Menno Sluzewski. 3d rotational angiography: the new gold standard in

the detection of additional intracranial aneurysms. *American Journal of Neuroradiology*, 29(5):976–979, 2008.

[87] Martin Vetterli. Multi-dimensional sub-band coding: Some theory and algorithms. *Signal processing*, 6(2):97–112, 1984.

[88] Quan Wang. Hmrf-em-image. `https://www.mathworks.com/matlabcentral/fileexchange/37530-hmrf-em-image`. Accessed: 2017-02-20.

[89] Quan Wang. Gmm-based hidden markov random field for color image and 3d volume segmentation. *arXiv preprint arXiv:1212.4527*, 2012.

[90] Weining Wang, Jiachang Li, Yizi Jiang, Yi Xing, and Xiangmin Xu. An automatic energy-based region growing method for ultrasound image segmentation. In *Image Processing (ICIP), 2015 IEEE International Conference on*, pages 1553–1557. IEEE, 2015.

[91] Yair Weiss. Segmentation using eigenvectors: a unifying view. In *Computer vision, 1999. The proceedings of the seventh IEEE international conference on*, volume 2, pages 975–982. IEEE, 1999.

[92] Koon-Pong Wong. Medical image segmentation: methods and applications in functional imaging. In *Handbook of biomedical image analysis*, pages 111–182. Springer, 2005.

[93] Zhenyu Wu and Richard Leahy. An optimal graph theoretic approach to data clustering: Theory and its application to image segmentation. *IEEE transactions on pattern analysis and machine intelligence*, 15(11):1101–1113, 1993.

[94] Xiaojiang Yang, Daniel J Blezek, Lionel TE Cheng, William J Ryan, David F Kallmes, and Bradley J Erickson. Computer-aided detection of

intracranial aneurysms in mr angiography. *Journal of digital imaging*, 24(1):86–95, 2011.

[95] Xin Yang, KT Tim Cheng, and Aichi Chien. Geodesic active contours with adaptive configuration for cerebral vessel and aneurysm segmentation. In *Pattern Recognition (ICPR), 2014 22nd International Conference on*, pages 3209–3214. IEEE, 2014.

[96] Zhong Yang, Yi Li, Weidong Chen, and Yang Zheng. Dynamic hand gesture recognition using hidden markov models. In *Computer Science & Education (ICCSE), 2012 7th International Conference on*, pages 360–365. IEEE, 2012.

[97] Sepideh Yazdani, Rubiyah Yusof, Alireza Karimian, Mohsen Pashna, and Amirshahram Hematian. Image segmentation methods and applications in mri brain images. *IETE Technical Review*, 32(6):413–427, 2015.

[98] Charles T Zahn. Graph-theoretical methods for detecting and describing gestalt clusters. *IEEE Transactions on computers*, 100(1):68–86, 1971.

[99] Tong Zhang, Yong Xia, and David Dagan Feng. Hidden markov random field model based brain mr image segmentation using clonal selection algorithm and markov chain monte carlo method. *Biomedical Signal Processing and Control*, 12:10–18, 2014.

[100] Yongyue Zhang, Michael Brady, and Stephen Smith. Segmentation of brain mr images through a hidden markov random field model and the expectation-maximization algorithm. *IEEE transactions on medical imaging*, 20(1):45–57, 2001.

[101] Barbara Zitova and Jan Flusser. Image registration methods: a survey. *Image and vision computing*, 21(11):977–1000, 2003.

Appendix: Visualization Tools

This section depicts a number of tools used to visualize the medical images data considered in this thesis.

- **Matlab:** MATLAB is a fully featured development environment for building sophisticated applications and user interfaces to execute models and algorithms and visualize and explore results. Therefore beside using Matlab for the algorithm implementation, it is used also to visualize the data in 2D and 3D as illustrated in figure 5.2. All figures reported in sections 4.3 and 4.3.1 are generated from Matlab.

- **Image Segmentation Application:** This application comes with the image processing toolbox in Matlab. It is used to investigate and preview different segmentation techniques (i.e, threshold-based, region growing, graph-cut, etc.) in one place as illustrated in figure 5.3. This application helped in generating the figures in section 2.1.

- **Gmsh:** It is a 3D mesh generator with built-in pre and post processing facilities. This software is used for the subjective evaluation phase in order to asses the segmentation performance. The main reason to use Gmsh instead of Matlab UI, is its 360° rotation feature. Figure 5.4 provides a screen shot from Gmsh software.

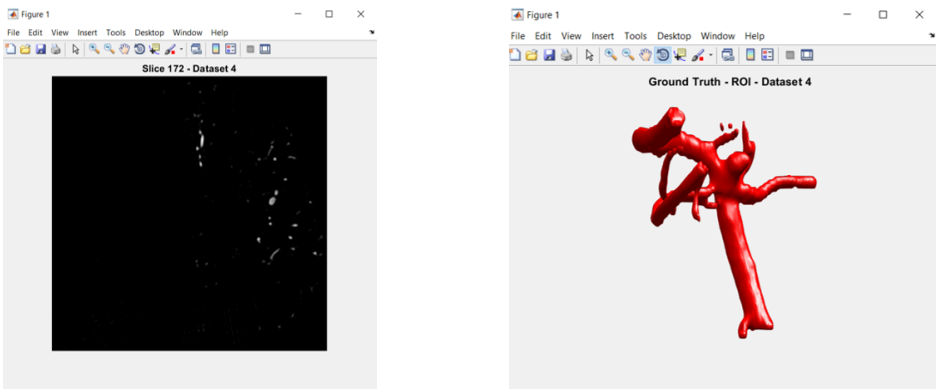

(a) (b)

Figure 5.2: A screen shot from the Matlab user interface (a) 2D slice (b) 3D volume

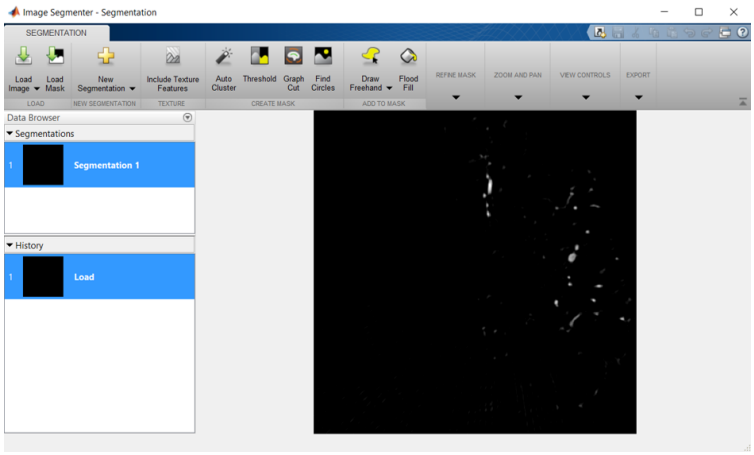

Figure 5.3: A screen shot from image segmentation application

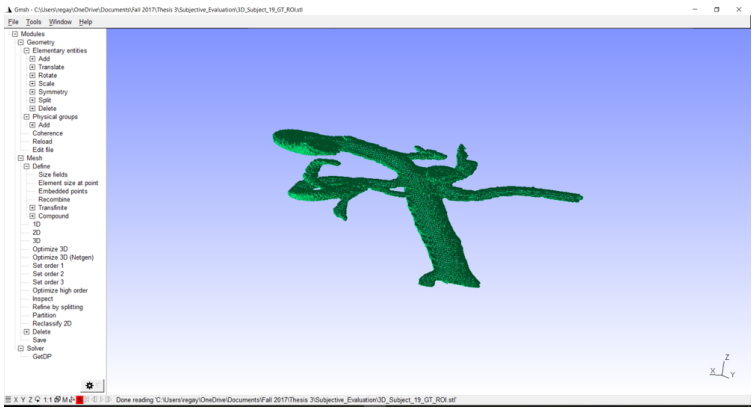

Figure 5.4: A screen shot from Gmsh software